



#### Available online at www.sciencedirect.com

# **ScienceDirect**

Geochimica et Cosmochimica Acta 224 (2018) 154-170

# Geochimica et Cosmochimica Acta

www.elsevier.com/locate/gca

# Cryogenic brines as diagenetic fluids: Reconstructing the diagenetic history of the Victoria Land Basin using clumped isotopes

Philip T. Staudigel<sup>a,\*</sup>, Sean Murray<sup>b</sup>, Daniel P. Dunham<sup>c</sup>, Tracy D. Frank<sup>c</sup>, Christopher R. Fielding<sup>c</sup>, Peter K. Swart<sup>a</sup>

Received 9 March 2017; accepted in revised form 3 January 2018; available online 11 January 2018

#### Abstract

The isotopic analyses ( $\delta^{13}$ C,  $\delta^{18}$ O, and  $\Delta_{47}$ ) of carbonate phases recovered from a core in McMurdo Sound by ANtarctic geologic DRILLing (ANDRILL-2A) indicate that the majority of secondary carbonate mineral formation occurred at cooler temperatures than the modern burial temperature, and in the presence of fluids with  $\delta^{18}O_{water}$  values ranging between -11 and -6% VSMOW. These fluids are interpreted as being derived from a cryogenic brine formed during the freezing of seawater. The  $\Delta_{47}$  values were converted to temperature using an in-house calibration presented in this paper. Measurements of the  $\Delta_{47}$ values in the cements indicate increasingly warmer crystallization temperatures with depth and, while roughly parallel to the observed geothermal gradient, consistently translate to temperatures that are cooler than the current burial temperature. The difference in temperature suggests that cements formed when they were  $\sim$ 260  $\pm$  100 m shallower than at the present day. This depth range corresponds to a period of minimal sediment accumulation from 3 to 11 Myr; it is therefore interpreted that the majority of cements formed during this time. This behavior is also predicted by time-integrated modeling of cementation at this site. If this cementation had occurred in the presence of these fluids, then the cryogenic brines have been a longstanding feature in the Victoria Land Basin. Brines such as those found at this site have been described in numerous modern highlatitude settings, and analogous fluids could have played a role in the diagenetic history of other ice-proximal sediments and basins during glacial intervals throughout geologic history. The agreement between the calculated  $\delta^{18}O_{water}$  value and the measured values in the pore fluids shows how the  $\Delta_{47}$  proxy can be used to identify the origin of negative  $\delta^{18}$ O values in carbonate rocks and that extremely negative values do not necessarily need to be a result of the influence of meteoric fluids or reaction at high temperature.

© 2018 Elsevier Ltd. All rights reserved.

Keywords: ANDRILL 2A; Antarctica; Cementation; Clumped isotopes; Cryogenic brines; Diagenesis; Isotope geochemistry; Victoria Land Basin

# 1. INTRODUCTION

The ANDRILL-2A (AND-2A) core, recovered from the Victoria Land Basin (VLB) in 2007–2008 (Fig. 1), penetrated over 1 km of Miocene to Recent glacially-derived

E-mail address: pstaudigel@rsmas.miami.edu (P.T. Staudigel).

<sup>&</sup>lt;sup>a</sup> Department of Marine Geosciences, University of Miami, Rosenstiel School for Marine and Atmospheric Sciences, 4600 Rickenbacker Causeway, Miami, FL 33149, USA

<sup>&</sup>lt;sup>b</sup> Department of Earth and Planetary Sciences, Macquarie University, Macquarie University, NSW 2109, Australia <sup>c</sup> Department of Earth & Atmospheric Sciences, 214 Bessey Hall, University of Nebraska-Lincoln, NE 68588-0340, USA

<sup>\*</sup> Corresponding author.

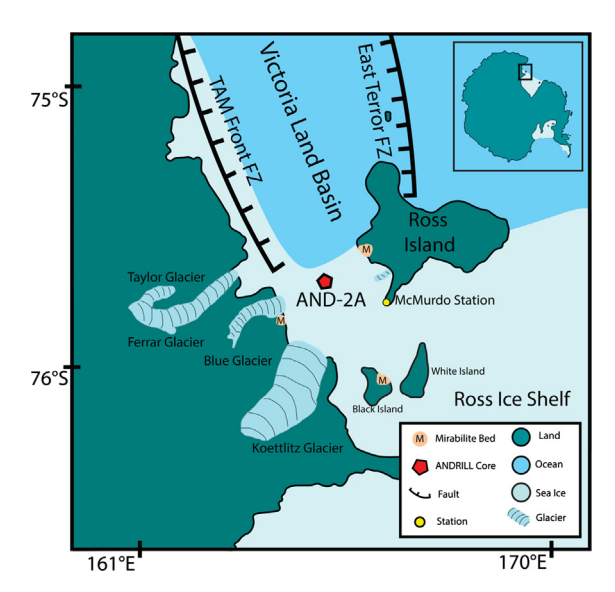


Fig. 1. Location map showing the AND-2A, relevant geologic features, mirabilite beds (Brady and Batts, 1981), Trans Antarctic Mountains Front Fault Zone (TAM Front FZ) and East Terror Fault Zone delineating the Victoria Land Basin (Paulsen and Wilson, 2009). Sea ice extent from LANDSAT image taken December 30, 2007.

siliciclastic sediment including diamictites, sandstones, and mudstones (Fielding et al., 2008a), recording the repeated advance and retreat of ice centers on the Antarctic continental margin (Fielding et al., 2011). These sediments are cemented by up to 25 wt.% carbonate consisting of calcite and dolomite. In addition, there are traces of detrital carbonate (Fig. 2a), biogenic carbonates (Fig. 2b), and carbonate fracture infills (Fig. 2d) (Paulsen et al., 2009). The uppermost sediments of the preserved succession are Pliocene to Modern in age. Between 75 and 200 m below seafloor (mbsf) there are several poorly constrained nondepositional surfaces which together account for a period of minimal sediment accumulation between 3 and 11 Ma. Sediments below 175 mbsf were deposited between 11 and 20 Ma with several pauses in sediment accumulation lasting up to 1.5 Myr, with a typical sediment accumulation rate of 10-20 cm/kyr (Acton et al., 2008; Levy et al., 2016).

During drilling, temperatures were recorded using a GyroSmart<sup>™</sup> core orientation tool; after each phase of drilling, the geothermal gradient was determined using a downcore logging tool (Wonik et al., 2008). While both methods give approximately the same geothermal gradient over the entire core, the measurements made during drilling are skewed towards the temperature of the drilling mud ( $\sim$ 20 °C) and thus tend to yield warmer shallow temperatures and cooler temperatures deeper in the core than the measurements obtained during logging (Schröder et al., 2011). Downcore temperatures were logged during several phases of drilling with subsequent measurements differing by less than 5 °C from those acquired previously. Temperatures measured during the final drilling phase (Phase 3) were utilized for this study since they had the longest time to equilibrate to ambient burial temperatures.

During core recovery, pore-waters were extracted from the sediments shortly after drilling (Panter et al., 2008). At depth, pore fluids had salinity values exceeding five times that of seawater, the  $\delta^{18}$ O values for these brines were as low as -11% relative to Vienna Standard Mean Ocean Water (VSMOW) (Fig. 3) (Frank et al., 2010). Elemental analyses of these fluids show a depletion in the concentration of sodium and sulfate relative to chloride, suggesting precipitation of the hydrated sodium sulfate mineral mirabilite (Na<sub>2</sub>SO<sub>4</sub>·10H<sub>2</sub>O) (Frank et al., 2010); this can be facilitated via batch freezing of seawater as the brineforming mechanism (Nelson and Thompson, 1954; Herut et al., 1990; Butler et al., 2016). Measurements of residual fluids from batch-freezing seawater laboratory and natural settings, have demonstrated that this freezing process results in a residual fluid with a more negative  $\delta^{\bar{1}8}\hat{O}$  value than the original seawater, differentiating them isotopically from evaporative brines (Horita, 2008; Toyota et al., 2013). This fractionation appears to follow an open-system Rayleigh relationship  $(R = R_0 f^{\alpha - 1})$  where the fractionation factor, α has been measured between 1.001 and 1.0025 (Toyota et al., 2013). As a result of their higher density, brines can be retained for thousands to millions of years (Lambert and Carter, 1984; Louvat et al., 1999; Bottomley et al., 2002, 2005).

Mirabilite deposits surrounding the Ross Sea (Fig. 1) suggest that these processes are common in the coastal areas adjacent to the Victoria Land Basin (Black and Bowser, 1967; Brady and Batts, 1981). Oxygen isotopic analyses of mirabilite deposits near Hobbs Glacier (location shown in Fig. 1) yielded  $\delta^{18}$ O values for Mirabilite-bound  $H_2O$  of -6.8 to -37.9% relative to SMOW for different samples, while sulfate  $\delta^{34}S$  values showed no significant difference to marine values and sulfate-bound oxygen yielded similar δ<sup>18</sup>O<sub>SO4</sub> values to sulfate in modern seawater (Bowser et al., 1970). Not all sulfate in mirabilite deposits in the area is derived from seawater however. Sun et al. (2015) describe mirabilite deposits further south, along the Lewis Cliff Ice Tongue, with more positive  $\delta^{34}$ S values of +49% and  $\delta^{18}O_{SO4}$  values around -22% relative to V-SMOW, the source of the sulfate was interpreted as having been derived from continental runoff. Although mirabilite is abundant in certain modern settings such as those described here, it is unlikely to be preserved beyond a few million years in the geologic record due to its high solubility and reactivity (Garrett, 2001), although there exist diagenetic pathways which can convert mirabilite to the unhydrated mineral theradonite (Na<sub>2</sub>SO<sub>4</sub>) (Herrero et al., 2015).

Two settings have been described in the literature wherein freezing water masses are isolated, allowing cryogenic brines to form and infiltrate into underlying sediment (Fig. 4). As continental-scale ice sheets advance into coastal settings, flexural troughs can form at their margins extending up to hundreds of kms (Walcott, 1970). Starinsky and Katz (2003) proposed that these isolated water masses froze over during the long timescales involved in the advance and retreat of ice sheets (Fig. 4a). Frank et al. (2010) hypothesize that this is the likely mechanism for producing the brines observed in the AND-2A core. Thermokarst lakes, a common feature at high latitudes, provide another mecha-

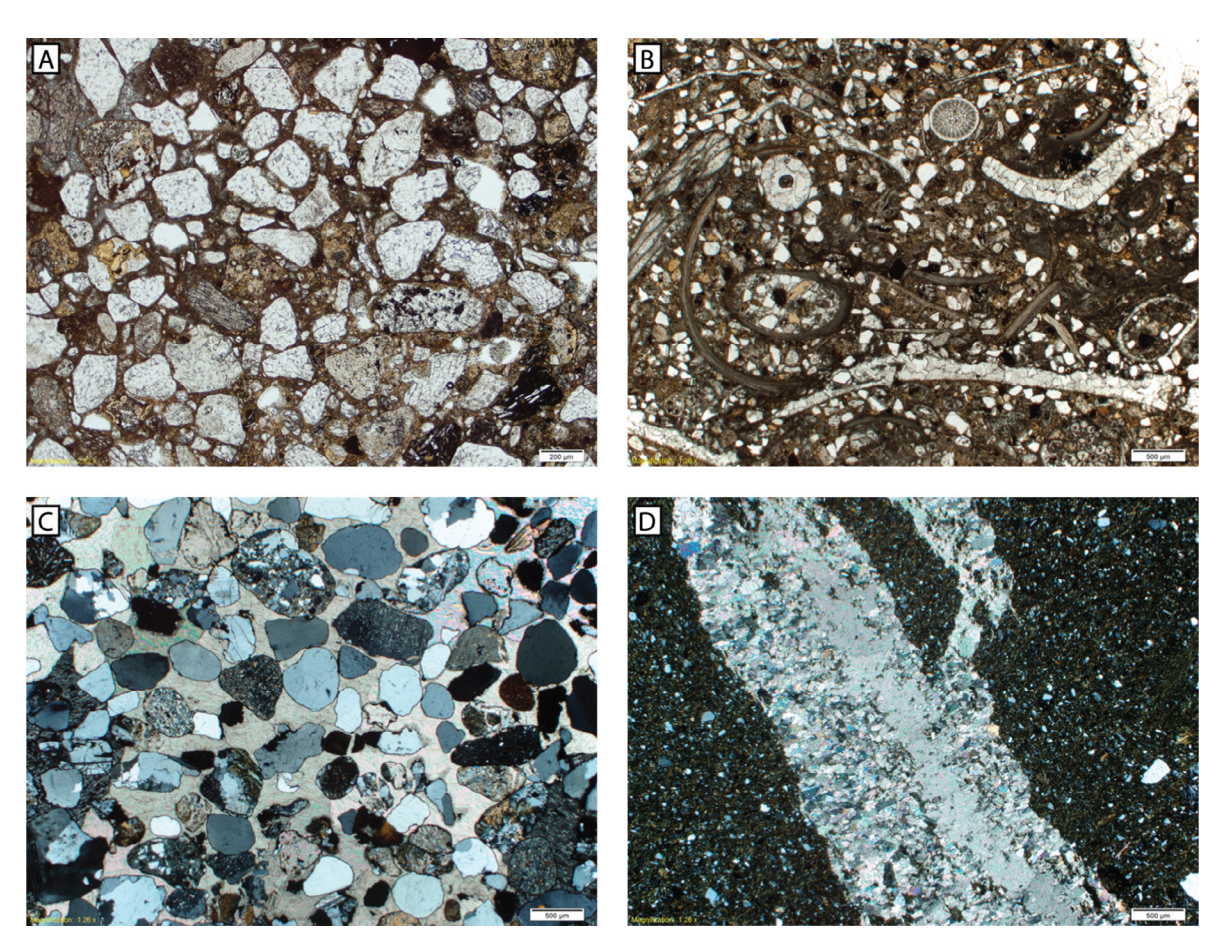


Fig. 2. (A) Lithic wacke with some marble clasts and minimal cement (223.20 mbsf), Plain Polarized Light (PPL). (B) Fossiliferous litharenite containing fragmented bryozoans, serpulid tubes, and echinoids, along with cement-filled molds after mollusk shells, inter-particle dolomite cement, PPL (616.36 mbsf). (C) Poikilotopic calcite cement in litharenite (808.67 mbsf), Crossed Polarized Lenses (XPL). (D) Calcite-filled fracture in siltstone, (958.7 mbsf) XPL.

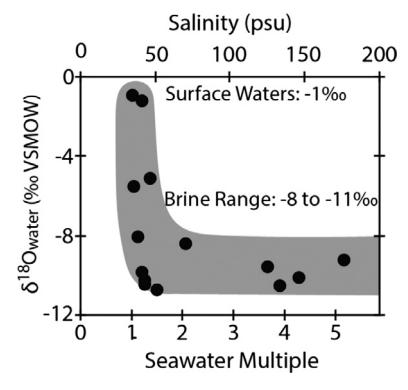


Fig. 3. Salinity and  $\delta^{18}O_{water}$  of brines recovered from the AND-2A Core by Frank et al. (2010). The  $\delta^{18}O_{water}$  values are plotted by depth in d.

nism for isolating seawater masses allowing brine and mirabilite to form as sea ice forms annually (Grasby et al., 2013) (Fig. 4b). It is likely in both settings that the resulting brine will infiltrate the pore space of underlying and adjacent sediments. Cryogenic brines have been described forming in the Ross Sea and McMurdo Sound area during sea

ice formation, often associated with brinicles or ice stalagmites (Paige, 1970; Dayton and Martin, 1971; Cartwright et al., 2013). The conditions necessary for brine formation could have existed in the region as early as the Oligocene, when Antarctica was periodically glaciated; although the extensively glaciated modern conditions have only been present since after the Miocene Climatic Optimum (MCO) (Kennett, 1977; Coxall et al., 2005; Barker et al., 2007; Galeotti et al., 2016).

Previous studies using biogenic carbonate phases in the AND-2A Core found evidence of extensive chemical alteration, including dissolution (Beu et al., 2014) and chemical exchange with pore fluid (Marcano et al., 2015). Cementation has been found to be highly variable in the AND-2A core, where vertically adjacent sedimentary units can display different degrees of cementation and cement types (Dunham et al., 2017). At depth, these cements, which can occlude virtually all porosity (Fig. 2c), show evidence of extensive recrystallization in the form of large crystals of cement enclosing sediment grains, termed poikilotopic cement, which indicate that recrystallization and cementation occur throughout their depositional history. Carbonate cements and other authigenic carbonate materials record increasingly more negative  $\delta^{18}$ O values with greater depth,

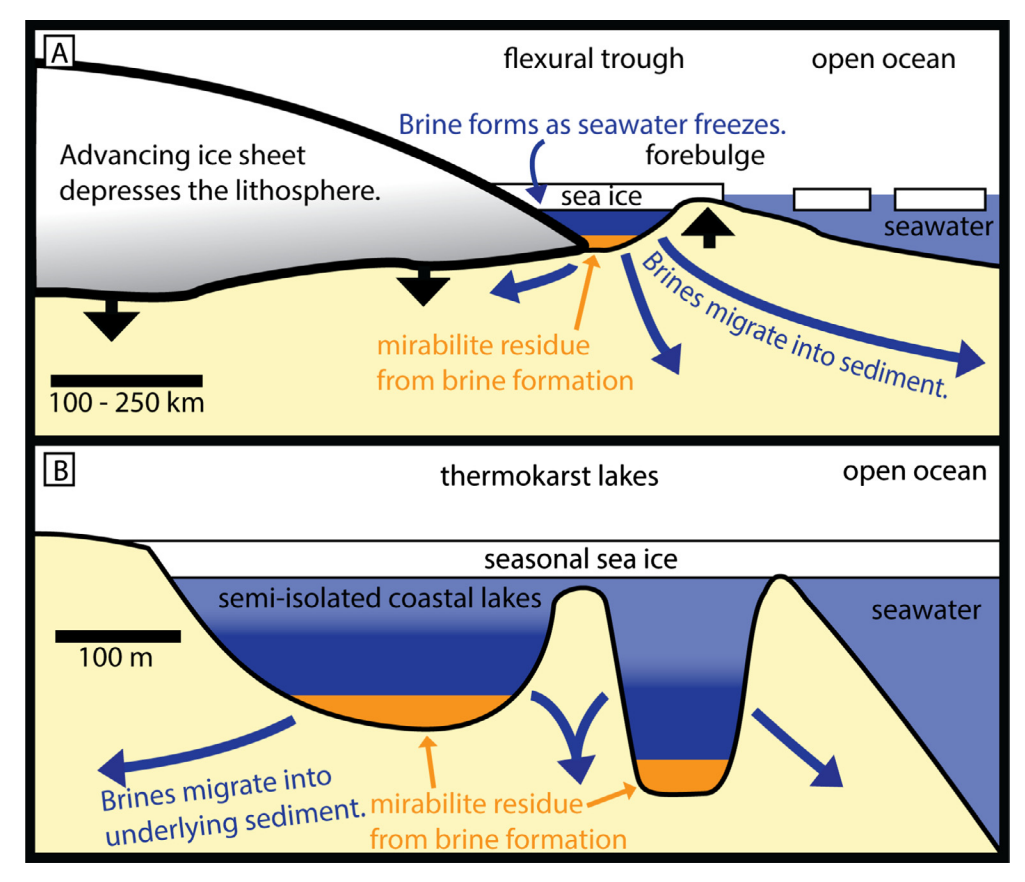


Fig. 4. Two geologic settings wherein cryogenic brine formation and mirabilite precipitation can occur. (A) Brine formation as seawater is isolated in a flexural trough caused by adjacent ice sheet depressing lithosphere, subsequent brines infiltrate underlying and adjacent sediment. Figure modified from Starinsky and Katz (2003). Approximately 10–20x vertical exaggeration. (B) Cryogenic brine formation as seawater is isolated and frozen in thermokarst lakes, figure modified from Grasby et al. (2013). Approximately 10x vertical exaggeration.

suggesting the involvement of these brines in the cementation history of the VLB (Fielding et al., 2012). Carbonate veins and fracture infills show negative  $\delta^{18}O$  values although with no significant trends downcore (Millan, 2013).

Traditionally, negative  $\delta^{18}O$  values in cements have been interpreted as being the result of meteoric diagenesis (Land and Epstein, 1970; Allan and Matthews, 1982; Burns and Matter, 1995) or later-stage cementation at higher burial temperatures (Engel et al., 1958; Salem et al., 2000). Cryogenic brines provide an alternative source of diagenetic fluids with negative  $\delta^{18}O$  values within high-latitude settings. The AND-2A core provides an excellent opportunity to study such processes as cementation at this site could have occurred over a considerable range of temperatures (–2 to +60 °C) due to the significant geothermal gradient (Wonik et al., 2008). Depending on the timing of carbonate precipitation, this would have resulted in considerable variation in the  $\delta^{18}O$  values of carbonates, independent of the water  $\delta^{18}O$  values.

In order to constrain this problem, an independent measure of temperature is needed. In this case we have used the  $\Delta_{47}$  proxy (Ghosh et al., 2006; Schauble et al., 2006; Eiler, 2011) which is insensitive to fluid composition and records the temperature of mineral formation provided that the

sample has not be subsequently reheated to >150 °C, at which point solid-state bond reordering may compromise the  $\Delta_{47}$  distribution (Passey and Henkes, 2012). Using this method, the average temperature of cementation (T $\Delta_{47}$ ) can be calculated, making it potentially a means of determining the burial depths at which authigenic minerals formed. The temperature determined with this method can then be combined with the conventional  $\delta^{18}$ O measurement of the carbonate minerals in order to determine the  $\delta^{18}$ O values of the fluid. The T $\Delta_{47}$  and fluid  $\delta^{18}$ O values can then be compared with knowledge of the existing geothermal gradient and the actual  $\delta^{18}$ O values of the pore fluids in order to determine the timing of cementation.

While there have been a number of equations which have related  $\Delta_{47}$  values to crystallization temperature (Ghosh et al., 2006; Dennis and Schrag, 2010; Tripati et al., 2010; Zaarur et al., 2013), recent equations (Tang et al., 2014; Kluge et al., 2015; Kelson et al., 2017) appear to be converging on a common calibration, even when using different acid digestion techniques and temperatures (Fernandez et al., 2017), similar to the calibration initially published by Dennis and Schrag (2010).

In this paper we present an additional calibration which supports these recently published equations. The calcium carbonate used in this calibration was synthesized in the laboratory at temperatures between 5 °C and 73 °C. These materials were analyzed for their  $\delta^{13}C,\,\delta^{18}O$  and  $\Delta_{47}$  values to create an in-house temperature calibration. The natural calcite and dolomite material from AND-2A was analyzed using the same analytical technique as the inorganic calibration carbonates, to calculate the temperature and  $\delta^{18}O_{water}$  values from which the minerals formed. These values have then been compared to measured burial temperatures and  $\delta^{18}O_{fluid}$  values that were measured during and after core recovery. Numerical simulations have been constructed to evaluate the burial and diagenetic history of these sediments, in particular the different rates of cementation and timing of brine infiltration are investigated for their effects on the final isotopic composition.

#### 2. MATERIALS AND METHODS

#### 2.1. Synthetic carbonate precipitation

Carbonates were synthesized at known temperatures (between 5 and 73 °C) via the reaction of calcium chloride (CaCl<sub>2</sub>) and sodium bicarbonate (NaHCO<sub>3</sub>) in de-ionized water as described in the following simplified reaction.

$$CaCl2 + 2NaHCO3 = CaCO3 + H2O + CO2 + 2NaCl (1)$$

Two methods were used to precipitate the carbonate, addition of NaHCO3 and CaCl2 simultaneously to DIW, or the addition of CaCl<sub>2</sub> to a DIW-NaHCO<sub>3</sub> solution. The second method was preferred at lower temperatures, as it enabled longer equilibration times for the dissolved carbonate species. Equilibration times can exceed several days at temperatures less than 15 °C (Beck et al., 2005). A 0.5 M solution of one or both reagents was titrated into a liter of DIW cooled to the experimental temperature at a rate of 20 µl per minute. The CO<sub>2</sub> was allowed to passively degas during the precipitation. In experiments where only CaCl<sub>2</sub> was titrated, the starting carbonate solution was a 0.01 mol/L solution of NaHCO<sub>3</sub>, equilibrated for several days prior to the addition of CaCl<sub>2</sub>. After precipitation is complete, the CaCO3-water mixture was centrifuged and the supernatant was decanted. Carbonate samples were dried overnight at 40 °C before being stored in glass scintillation vials prior to isotopic analysis. The water used was analyzed for its δ<sup>18</sup>O value using a Picarro™ L2140-i cavity ring-down spectrometer.

#### 2.2. Selection and preparation of AND-2A carbonates

The AND-2A core consists predominantly of siliciclastic sediments derived from either glacial or pelagic sources (Fielding et al., 2008a). Petrographic analysis by Dunham et al. (2017), determined that cements were principally calcite or dolomite. Other secondary minerals, such as zeolites, sulfides and silicates, have also been found as cements and fracture infills along with the carbonates (Paulsen et al., 2009). The carbonate samples described in this study were determined by Fielding et al. (2011, 2012) to have formed either as primary (biogenic) material or secondary cements and fracture infills. The biogenic materials selected for anal-

ysis showed petrographic evidence for nearly complete recrystallization (Fig. 2b). Mineralogy was determined using petrographic techniques and confirmed using X-ray Diffractometry.

Bulk sediment samples (n=18), biogenic carbonates (n=5), and vein carbonates (n=2), collected between 150 and 1083 mbsf were selected for analysis. Bulk sediment samples were broken apart and powdered using a ball grinder. Biogenic and vein carbonates were drilled with a UP201C rotary tool using an Axis Dental Part: H1-008HP drill bit, using the minimum possible drill RPM to reduce heating and alteration (Staudigel and Swart, 2016). The sediment matrix from 616.36 mbsf, where biogenic materials were abundant, was sampled using the same drilling technique, avoiding shells and worm casings. The barnacle at 158.80 mbsf was in a poorly-lithified diamictite, and was extracted using a metal probe before being ground in a mortar and pestle. Samples not analyzed immediately were stored in Eppendorf tubes.

## 2.3. Isotopic analysis

While under normal circumstance each measurement of the  $\Delta_{47}$  value requires  $\sim 8$  mg of carbonate in order to produce sufficient CO2 for analysis, because the sediments in the VLB are predominantly siliciclastic and therefore have low carbonate fractions (F<sub>carbonate</sub>), up to 150 mg of sediment was necessary for each analysis (required mass = 8mg/F<sub>Carbonate</sub>). Samples were weighed into copper reaction boats and reacted using the common acid bath at 90 °C, using concentrated phosphoric acid (density = 1.95 g/cc) on the University of Miami Stable Isotope Laboratory's vacuum line. It is assumed that the detrital material, which was predominantly sand and clays, did not react to form CO2 or other isobarically interfering gases, and did not affect the reaction of cements with phosphoric acid. Liberated gas was continuously frozen with liquid nitrogen in a U-trap throughout the duration of reaction in order to minimize the potential of exchange between CO2 and water released from reaction with acid or adhered to clay. Calcite samples reacted to completion within 30 min, dolomite samples required longer reaction times, typically reacting for 45 min to 1 h before bubbles were no longer produced. Reaction times were apparently unaffected by carbonate content. The H<sub>2</sub>O was separated from CO<sub>2</sub> using a -90° C methanol slush. Volatile organic compounds and other contaminants were removed by passing the gas through a Porapak™ Q adsorbent trap (passively, no He carrier gas) chilled in methanol between -20 and -30 °C, gas was frozen in a trap cooled with LN<sub>2</sub> after passing through to facilitate 100% extraction of gas. Gas samples are frozen into a glass vessel and transferred to a Thermo-253 mass spectrometer. Samples were measured at a mass-44 beam intensity of 12 V, relative to an in-house working gas, calibrated relative to NBS-19 (National Bureau of Standards) standard. In order to facilitate a pressure baseline correction (He et al., 2012), all samples were analyzed 14x "on peak" bracketed by four analyses "off peak", the "off peak" baseline value a was subtracted from the "on peak" value in order to adjust for this non-zero baseline on the mass-47 cup. Each block of measurements taking 30 min; these blocks of measurements were repeated six times.

#### 2.4. Data processing

Carbon and oxygen isotope values for solids are reported relative to the Vienna Pee Dee Belemnite Standard (VPDB) using the conventional delta notation. The  $\delta^{18}$ O values were corrected for acid fractionation at 90 °C in a common acid bath following the equation published by Swart et al. (1991).

Clumped isotope values for all samples and reference materials are calculated using the methods outlined by (Huntington et al., 2011) using a value for  $\lambda$  of 0.528 (Barkan and Luz, 2005) and revised abundances for PDB  $^{13}\text{C}/^{12}\text{C}$  (Chang and Li, 1990),  $^{17}\text{O}/^{16}\text{O}$  (Assonov and Brenninkmeijer, 2003) and  $^{18}\text{O}/^{16}\text{O}$  (modified from Baertschi, 1976), following the Brand et al. (2010) parameters as recommended for use in the calculation of  $\Delta_{47}$  values by Daëron et al. (2016).

Data were adjusted into the absolute reference frame outlined by Dennis et al. (2011) by analyzing equilibrated CO<sub>2</sub> relative to a working gas. Carbon dioxide equilibrated with water at 25 °C ( $\Delta_{47} = 0.925\%$ ) and 50 °C ( $\Delta_{47} =$ 0.805‰), as well as  $CO_2$  heated in a quartz tube at 1000  $^\circ$ C ( $\Delta_{47} = 0.027\%$ ) were used as standard gases with known clumped isotope distributions whose values are calculated from Wang et al. (2004) as shown in Dennis et al. (2011). Three gases of variable composition were used in order to correct for any mass-dependent effects between measured  $\delta^{47}$  and  $\Delta_{47}$  values, CO<sub>2</sub> liberated from a Carrara marble via phosphoric acid digestion was used heated to 1000 °C and used as a fourth gas. Linear interpolation of the slopes and intercepts of measured  $\Delta_{47}(\text{raw})$  and  $\delta^{47}(\text{relative to})$ working gas) values of suites for heated and equilibrated gases analyzed on different days allowed for any instrumental drift to be corrected for. Daily analyses of a Carrara marble yielded a  $\Delta_{47}$  value of 0.392%  $\pm$  0.027 (n = 443) in the absolute reference frame (Murray and Swart, 2017). All relevant data are included in the supplemental material.

Both calcite and dolomite samples have been analyzed for their  $\Delta_{47}$  values in this study. Whilst the determination of temperatures in calcite using  $\Delta_{47}$  values is reasonably mature, there has been uncertainty regarding the appropriate equations to use for dolomite (Defliese et al., 2015; Murray, 2016; Bonifacie et al., 2017). For example, the recent equation for dolomite proposed by Bonifacie et al. (2017), although similar to the group of equations recently proposed for calcite within the calibration range of this study, is diverges at higher temperatures, suggesting that there may be a difference between calcite and dolomite. Alternatively, the difference may be part of an evolving understanding of temperature- $\Delta_{47}$  relationships. Similarly, there has been some controversy about the application of mineral-specific acid fractionation factors. It has been suggested by some workers that the commonly used value for reaction at 90 °C of +0.092% for calcite (Passey et al., 2010) is also applicable to dolomite, while in other studies values as high as +0.153\% have been proposed (Murray

et al., 2016). In this study, we have used an acid fractionation factor of +0.092‰ for calcite and 0.153‰ for dolomite as these values were determined under identical conditions and methods to the samples measured in this study. We also note that this difference between calcite and dolomite has been observed in samples prepared using a Kiel autocarb device at ETH (Müller et al., 2017). The precise cause of this discrepancy is not determined, however because this study uses identical sample preparation to Murray et al. (2016), their method for determining paleotemperature is used, although the approach of Bonifacie et al. (2017) is discussed further in Section 4.2.

The  $\delta^{18}$ O values of the waters from which carbonates were formed ( $\delta^{18}$ O<sub>water</sub>) were calculated using the temperatures derived from  $\Delta_{47}$  values ( $T\Delta_{47}$ ) and the  $\delta^{18}$ O values of the carbonates ( $\delta^{18}$ O<sub>carbonate</sub>) for each replicate analysis. Temperature- $\delta^{18}$ O relationships were used for calcite (Kim and O'Neil, 1997) and dolomite (Matthews and Katz, 1977), following the recommendations of Murray and Swart (2017). The relationship for Kim and O'Neil (1997) was revised using the acid fractionation factor for sealed vessel reaction at 25 °C ( $\alpha$  = 1.01025) calculated from Swart et al. (1991), rather than the value of 1.01050 obtained by Sharma and Clayton (1965). Samples which were mixtures of calcite and dolomite were processed using intermediate acid fractionation factors and temperature- $\delta^{18}$ O relationships.

#### 2.5. Statistical methods

Covariance is calculated using least-squares linear fits, where significance is determined using a *p*-from-*r* calculation assuming a normal distribution. A *t*-value for linear fit is calculated using the Fisher method.

$$t = \frac{r}{\sqrt{(1 - r^2)/(N - 2)}}\tag{2}$$

When comparing the difference between two linear regressions, significance is calculated from the residual of the two regressions. Significance is defined as having less than 1% chance (p < 0.01) of being the result of a random distribution. In figures where linear regressions are plotted, 95% certainty for linear fit is displayed ( $\alpha = 0.05$ ).

#### 2.6. Time-integrated modeling

A time-integrated model was used to evaluate the effects of different cementation histories on the eventual  $\Delta_{47}$  and  $\delta^{18}O$  values of cements. This approach, previously demonstrated to have utility in describing the diagenetic behavior of  $\delta^{18}O$  (Schrag et al., 1995) and  $\delta^{34}S_{CAS}$  (Rennie and Turchyn, 2014) in carbonates, was applied in this study to describe the behavior of  $\Delta_{47}$  values during cementation. This model simulates the sedimentation history by breaking it into intervals of 100 kyr. Over each time step, a package of sediment was added to the top of the sediment column, the thickness of which was calculated using an age-depth model modified from Levy et al. (2016). Down core temperatures were calculated based on the published geothermal gradient from Wonik et al. (2008). Downcore  $\delta^{18}O_{water}$  val-

ues were calculated using a brine  $\delta^{18}O$  value of -10% (SMOW) derived from the median brine value from Frank et al. (2010), and a non-brine value of -1% from the surface  $\delta^{18}O_{water}$  value given in the same reference. The brine value was used below 50 mbsf after the time of brine emplacement, which varied between models. Carbonate cement was added downcore at equilibrium with the burial temperature and porewater  $\delta^{18}O$  values. The models simulated rates of cementation using a conventional exponential decay function

$$R = A + B * e^{-\text{age/C}} \tag{3}$$

in which A corresponds to a constant rate of diagenesis  $(\text{myr}^{-1})$ , B corresponds to the rate of an initial pulse in cementation  $(\text{myr}^{-1})$ , C is the decay rate of the initial pulse (myr). Three simulations were run, modeling possible behaviors of cementation rate. The first simulation ("Pulse") models an initial cementation pulse which decays over time to zero (A=0, B=1, C=2000 kyr), the second ("Pulse + Constant") models an initial pulse of cementation (B=0.8, C=2000 kyr) which decays to a slower rate over time (A=0.2). The third simulation ("2x Brine Rate") models a constant cementation rate (B=0), however the cementation rate is doubled in the presence of brines.

Each of these rate models were run six times with brine emplacement ranging between modern and 20 Ma in increments of 4 myr. Cements form at equilibrium with respect to ambient temperature and the water  $\delta^{18}O$  value, and are modeled using the temperature- $\alpha_{water-calcite}$  relationship modified from Kim and O'Neil (1997). The displayed simulation outputs are the final  $T\Delta_{47}$ , and  $\delta^{18}O_{water}$  values for bulk cement.

Because adjacent sediment packages can experience different rates and degrees of cementation (Dunham et al., 2017), it is necessary to implement several rate models in order to describe the range of potential diagenetic histories for this site.

# 3. RESULTS

# 3.1. Synthetic carbonate composition

The  $\delta^{13}C$ ,  $\delta^{18}O$  and  $\Delta_{47}$  values of all synthetic carbonates are displayed in Table 1. A weighted regression

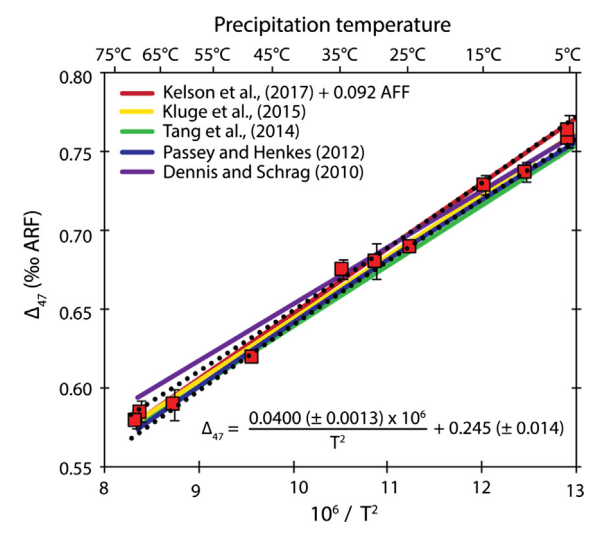


Fig. 5.  $\Delta_{47}$  values ( $\pm 1$  st. error) of synthetic carbonates plotted relative to temperature of precipitation. Dotted lines show 95% CI for linear regression. Linear regressions for Temperature  $-\Delta_{47}$  calibrations from previous studies are plotted as solid colored lines. An Acid Fractionation Factor (AFF) of +0.092 is applied to Kelson et al. (2017)'s slope.

through the  $\Delta_{47}$  values for synthetic carbonates relative to the known temperatures (Fig. 5) of precipitation yields the significant ( $r^2 = 0.96$ , n = 44) linear relationship shown in Eq. (4).

$$\Delta_{47} = \frac{0.0400(\pm 0.0013) \times 10^6}{T^2} + 0.245(\pm 0.014) \tag{4}$$

The fractionation of oxygen isotopes and water is described using the following relationship, displayed in Fig. 6.

$$1000 ln \alpha_{water-calcite} = 18.73 (\pm 0.39) \frac{10^3}{T} - 34.17 (\pm 1.29)$$
 (5)

Most of the precipitation experiments conducted herein were precipitated between 10 and 15 mM DIC, except for one 5 °C experiment, which was run at  $\sim$ 35 mM and sits well above the linear regression for the other samples, although it's  $\Delta_{47}$  values are not significantly different than

Table 1
Precipitation temperatures, mineralogy and isotopic composition of the 11 synthetic carbonates used in this study as well as the isotopic composition of water from in which each precipitation experiment was conducted.

Precipitation temperature (°C)	Mineralogy	δ <sup>13</sup> C (‰ VPDB)	δ <sup>18</sup> O (‰ VPDB)	$\Delta_{47}$ (% ARF)	N	δ <sup>18</sup> O <sub>water</sub> (‰ VSMOW)
5	Calcite	$-11.72 \pm 0.09$	$3.06 \pm 0.03$	$0.759 \pm 0.011$	3	-0.65
5	Calcite	$-14.23 \pm 0.13$	$2.34 \pm 0.06$	$0.764 \pm 0.016$	3	-0.59
10	Calcite	$-12.89 \pm 0.06$	$0.76 \pm 0.13$	$0.737 \pm 0.010$	3	-0.45
15	Calcite	$-13.09 \pm 0.04$	$0.27 \pm 0.08$	$0.729 \pm 0.015$	7	-0.40
25	Calcite	$-13.14 \pm 0.04$	$-2.31 \pm 0.12$	$0.690\pm0.004$	3	-0.47
30	Calcite	$-12.14 \pm 0.01$	$-3.08 \pm 0.08$	$0.681 \pm 0.020$	3	-0.27
35	Calcite	$-8.33 \pm 0.34$	$-3.94 \pm 0.10$	$0.676 \pm 0.015$	6	-0.25
50	Calcite	$1.43 \pm 0.06$	$-6.78 \pm 0.05$	$0.620 \pm 0.006$	4	-0.40
65	Calcite	$-13.49 \pm 0.03$	$-9.38 \pm 0.11$	$0.590 \pm 0.021$	5	-0.10
72	Aragonite	$-13.21 \pm 0.11$	$-9.91 \pm 0.06$	$0.585 \pm 0.012$	3	0.46
73	Aragonite	$-12.85 \pm 0.28$	$-9.77 \pm 0.12$	$0.581\pm0.011$	4	-0.42

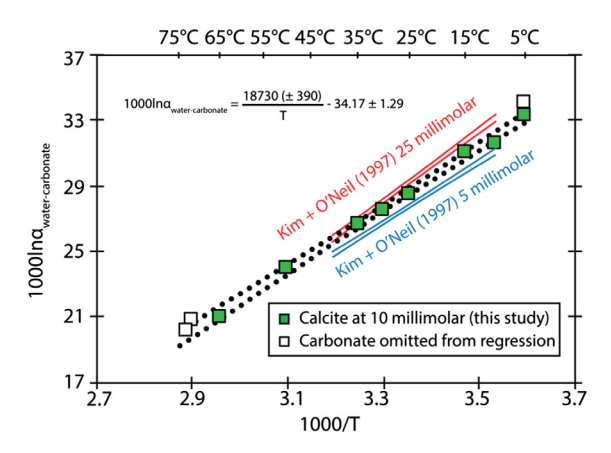


Fig. 6.  $1000 \ln \alpha_{water-calcite}$  for all inorganic precipitates relative to temperature of precipitation. Linear regression calculated using calcites precipitated at 10 mM DIC concentration (filled squares). Stippled lines dilineate uncertainty for linear regression ( $\pm 95\%$  CI). Two linear relationships modified from Kim and O'Neil are displayed for experiments conducted at 5 mM and 25 mM DIC concentration between 15 and 40 °C.

a sample precipitated from a lower DIC concentration (Fig. 5). This sample was omitted from linear regression for Eq. (5). The two highest temperature experiments, were omitted from Eq. (5) because they consisted predominantly of aragonite, which fractionates oxygen isotopes differently than calcite during precipitation (Grossman and Ku, 1986; Kim et al., 2007). These three samples were, however, still used in the linear regression for  $\Delta_{47}$ .

# 3.2. Isotopic composition of AND-2A carbonates

The compositions of all carbonate materials described herein are displayed in Table 2.

### 3.2.1. Bulk sediments/cements

The majority of carbonates analyzed in this study were composed of either calcite or dolomite, two samples (616.36 and 730.45 mbsf) contained roughly equal mixtures of calcite and dolomite (Fig. 2b). The  $\delta^{13}$ C values of the carbonate cements range between -30% and 0%, with all but three samples falling between -10% and 0%(Fig. 7a). Dolomite cements'  $\delta^{13}$ C values averaged -4.1 $\pm$  2.2%, while calcite was more negative and variable, averaging  $-12.3 \pm 8.7\%$ . With increasing depth, the cements record progressively more negative δ<sup>18</sup>O values, reaching a broad minimum below 700 mbsf at approximately -9%c  $\pm$  2% (Fig. 7b). This trend is also recorded in T $\Delta_{47}$  values, which range between 1.0 °C and 43.1 °C (Fig. 7c). The  $\delta^{18}$ - $O_{water}$  values calculated using  $\delta^{18}O_{carbonate}$  values and temperatures from  $\Delta_{47}$  values ranged between +2.6 and -11.5%, with the majority of samples between -5% and -10%c.

# 3.2.2. Biogenic materials

All biogenic materials were comprised of calcite, even in instances where cement mineralogy was dolomite. Biogenic carbonates' isotopic compositions varied less than those of cements, with  $\delta^{13}C$  values ranging between -1.7% and -9.3% VPDB. Carbonate  $\delta^{18}O$  values ranged between -2.22% and -8.12% VPDB. Temperatures estimated from  $\Delta_{47}$  values varied between  $-5.0\,^{\circ}C$  and  $33.1\,^{\circ}C$ , yielding  $\delta^{18}O_{water}$  values of between -5.2% and -8.9% VSMOW. Reconstructed fluid  $\delta^{18}O$  values and carbonate  $\delta^{13}C$  values covary significantly in all biogenic materials (Fig. 8), ranging between the "pristine" material described by Levy et al. (2016) and the average  $\delta^{18}O$  and  $\delta^{13}C$  values of the pore fluid.

There is no significant relationship between the  $\delta^{13}$ C values of the biogenic materials and the corresponding cements (Fig. 9a, p=0.286). The  $\delta^{18}O_{\rm carboante}$  values of the measured biogenic materials co-vary significantly (p=0.006, Fig. 9b) with the  $\delta^{18}O_{\rm carbonate}$  values of corresponding matrix cements, but are more negative by  $0.5\%c \pm 0.3\%c$ . A similar co-variance is observed in the  $\Delta_{47}$  values (Fig. 9c), although it is not highly significant (p=0.055), temperatures also do not display a significant offset. There is no significant covariance between  $\delta^{18}O_{\rm water}$  values of biogenic materials and their respective cements (Fig. 9d). A bivalve sample collected at 616.36 mbsf, which was in a dolomite cemented matrix (Fig. 2b), was the most compositionally offset from its matrix, recording cooler temperatures, and more positive  $\delta^{13}C$  and  $\delta^{18}O$  values.

#### 3.2.3. Vein carbonates

The two vein carbonates sampled in this study were compositionally distinct from one another, they were sampled from a similar burial depth approximately 10 m apart (958.70 and 968.96 mbsf). The vein sampled at 958.70 was comprised of calcite spar (Fig. 2d) with an extremely negative  $\delta^{13}$ C value ( $\sim$ -15%), while the other was dolomite and had a more positive  $\delta^{13}$ C value (+1%) than any overlying dolomite cements (Table 2, Figs. 7, 8). The  $\delta^{18}$ O values for both samples were relatively negative: -12.7% for calcite and -10.2% for dolomite. The temperature calculated using  $\Delta_{47}$  values were 30 °C and 48 °C for the calcite and dolomite veins, respectively. These temperatures, when used in conjunction with  $\delta^{18}$ O<sub>carbonate</sub> values, calculate  $\delta^{18}$ O<sub>fluid</sub> values of -9.2% and -5.8% relative to VSMOW.

#### 3.3. Model output

All iterations for a given rate model produced identical  $T\Delta_{47}$  values. The  $T\Delta_{47}$  output for the "Pulse", "Pulse + Constant", and "2x brine rate" models are plotted in Fig. 10a, along with measured burial temperatures (Wonik et al., 2008) and  $T\Delta_{47}$  for carbonates measured in this study. The "Pulse" model invariably produced the coolest  $T\Delta_{47}$  estimates and the "2x brine rate" model produced the warmest  $T\Delta_{47}$  values, which were approximately parallel, but offset from the measured burial temperatures. The "Pulse + Constant" model is intermediate to the other two models. All models showed a significant shift in  $T\Delta_{47}$ and δ<sup>18</sup>O<sub>water</sub> values between 100 and 200 mbsf which corresponded to a slowing of sediment accumulation in the age-depth model. Earlier times of brine emplacement invariably record more significant incorporation of negative  $\delta^{18}O_{\text{water}}$  values into cements (Fig. 10b-d).

Table 2 Isotopic composition of carbonate materials analyzed in this study.  $\Delta_{47}$  values are adjusted for reaction at 90 °C using an acid fractionation factor of +0.092% for Calcite (Passey et al., 2010) and +0.153% for dolomite (Murray et al., 2016).

ANDRILL 2A	isotope analyses											
Depth (mbsf)	Sample type	Number of replicate analyses	δ <sup>13</sup> C VPDB (‰)	std. dev	δ <sup>18</sup> O VPDB (‰)	std. dev	$\Delta_{47}~(\% o)$	std. dev	TΔ <sub>47</sub> (°C)	std. dev	δ <sup>18</sup> O <sub>water</sub> (‰ VSMOW)	std. dev
Biogenic mater	rials (all calcite)											
158.8	Barnacle shell	2	-2.898	0.048	-2.217	0.203	0.802	0.005	-5.0	1.3	-5.9	0.5
377.54	Bivalve shell	2	-8.604	0.511	-6.783	0.285	0.772	0.000	2.5	0.1	-8.9	0.3
377.54	Worm tube	3	-9.290	1.008	-6.806	0.397	0.757	0.006	6.4	1.7	-8.0	0.6
616.36	Bivalve shell	2	-1.705	0.088	-8.115	0.283	0.694	0.001	25.5	0.4	-5.2	0.2
968.53	Bivalve shell	2	-7.345	0.126	-11.627	0.391	0.673	0.030	33.1	10.9	-7.5	2.5
Fracture infills												
958.7	Calcite	2	-15.362	0.083	-12.786	0.095	0.679	0.020	30.5	6.9	-9.2	1.5
968.96	Dolomite	2	0.943	0.649	-10.160	0.146	0.632	0.004	48.2	1.6	-5.8	0.5
Carbonate cem	ents											
215.49	Calcite	3	-4.986	0.117	-5.711	0.511	0.778	0.020	1.0	5.2	-8.1	1.1
223.2	Calcite + marble (?)	3	-28.489	0.074	-2.882	0.142	0.660	0.012	37.4	4.4	2.6	0.7
350.07	Calcite	2	-6.066	0.242	-6.346	0.293	0.750	0.008	8.4	2.3	-7.0	0.2
377.54	Calcite	2	-5.769	0.014	-6.426	0.636	0.753	0.001	7.6	0.2	-7.3	0.6
409.64	Dolomite	4	-2.823	0.126	-6.112	0.294	0.728	0.008	14.7	2.3	-8.9	0.7
458.3	Dolomite	2	-6.663	0.383	-5.489	0.203	0.756	0.030	6.8	8.1	-10.4	2.5
462.33	Dolomite	2	-4.898	0.126	-5.729	0.745	0.733	0.029	13.4	8.6	-8.8	3.0
465.53	Dolomite	2	-5.154	0.157	-5.277	0.183	0.737	0.003	12.0	0.9	-8.7	0.4
482.77	Calcite	3	-21.554	0.424	-9.117	0.295	0.756	0.012	6.8	3.4	-10.4	1.0
625.07	Dolomite	2	-3.696	0.011	-6.605	0.488	0.695	0.031	25.2	10.2	-6.9	2.9
616.36	Calcite + dolomite	3	-3.466	1.898	-7.268	1.193	0.717	0.022	18.3	7.0	-7.5	1.3
633.11	Dolomite	3	0.512	0.097	-7.915	0.222	0.737	0.006	12.0	1.6	-11.5	0.7
718.22	Calcite	3	-15.552	0.037	-11.850	0.093	0.677	0.023	31.5	8.4	-8.0	1.6
728.99	Dolomite	2	-5.067	0.152	-8.745	0.316	0.645	0.012	43.1	4.7	-5.3	0.6
730.45	Calcite + dolomite	2	-3.469	0.126	-6.915	0.453	0.708	0.026	21.1	8.2	-6.5	2.3
791.13	Calcite	2	-6.324	0.379	-9.763	0.062	0.670	0.010	33.7	3.6	-5.3	0.6
968.53	Calcite	2	-7.684	0.038	-11.337	0.300	0.672	0.001	32.9	0.4	-7.2	0.2
1093.61	Calcite	2	-6.706	0.045	-10.178	0.205	0.682	0.010	29.4	3.3	-6.6	0.9

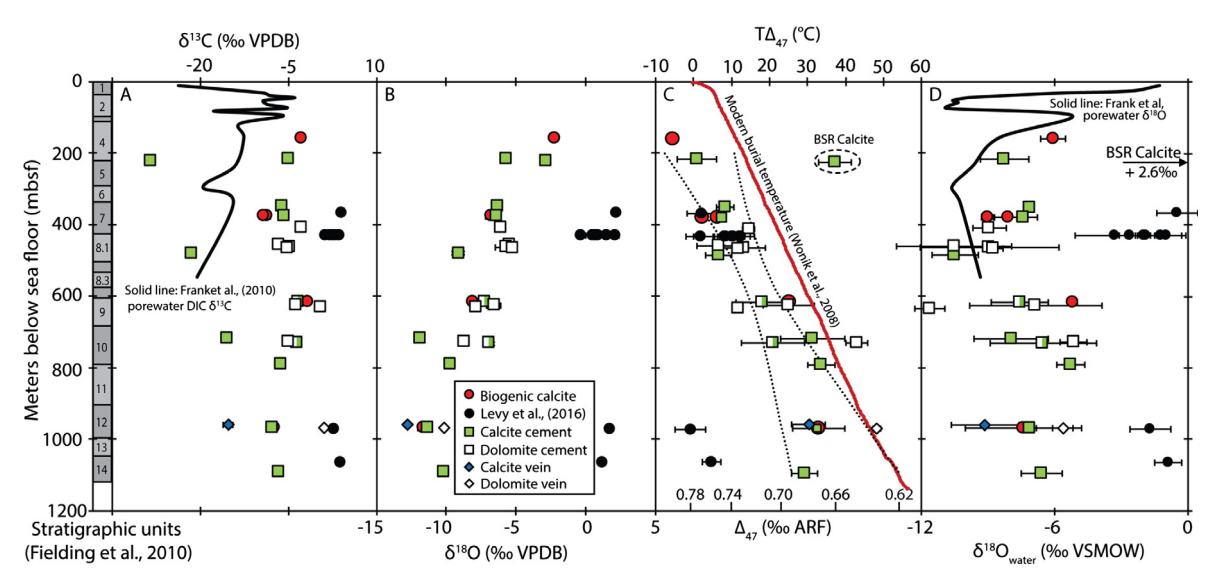


Fig. 7. Plots for ANDRILL 2A calcite (filled symbols), dolomite (white symbols) and mixed calcite/dolomite (half white) carbonate isotopic compositions of cements (squares), biogenic calcite (circles) and carbonate veins (diamonds) relative to downcore depth. Unaltered biogenic materials described by Levy et al. (2016) are plotted as solid black dots, temperatures and interpreted  $\delta^{18}O_{\text{water}}$  values are taken from the original text. A:  $\delta^{13}C$  of carbonates and Frank et al. (2010)'s porewater DIC  $\delta^{13}C$  plotted as solid line. B:  $\delta^{18}O_{\text{carbonate}}$ . C:  $\Delta_{47}$  and interpreted temperatures from carbonate, and modern burial temperatures measured during logging (Wonik et al., 2008) plotted as solid line. Dotted lines: 95% confidence of linear regression through all cements. Calcite interpreted to have formed from bacterial sulfate reduction are circled and labeled BSR Calcite. D:  $\delta^{18}O_{\text{water}}$  calculated from plots B and C. Measured brine  $\delta^{18}O$  from Frank et al. (2010) is plotted as a solid line.

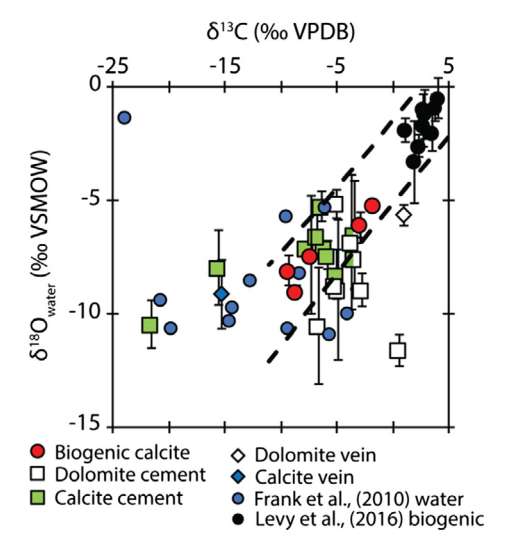


Fig. 8.  $\delta^{13}C_{DIC}$  and  $\delta^{18}O_{water}$  of pore fluids described by Frank et al. (2010), plotted with the  $\delta^{13}C_{carbonate}$  and  $\delta^{18}O_{water}$  reconstructed with clumped isotopes of the carbonate materials measured in this study and by Levy et al. (2016). Half-filled squares are mixtures of dolomite and calcite cement. Dashed lines illustrate  $\pm 95\%$  CI of linear regression through all biogenic material.

The recorded  $\delta^{18}O_{water}$  value calculated from  $\Delta_{47}$  values varied with different times of brine emplacement and are plotted in Fig. 10b–d. In models incorporating early brine emplacement (e.g. 20 Ma), the brine  $\delta^{18}O$  value has a greater impact on the resulting cements than models where brine is emplaced later in the depositional history. In the "Pulse" model, cement composition is biased towards earli-

est burial conditions, directing it towards cooler temperatures (Fig. 10a), and more positive reconstructed fluid  $\delta^{18}O$  values, necessitating earlier times of brine emplacement in order to record the negative oxygen isotope composition. In the "Pulse + Constant" model (Fig. 10c), the output cement  $\delta^{18}O_{water}$  values are more positive than those of the "Pulse" model, with greater linear downcore trends. The "2x brine rate" model (Fig. 10d) yields cements with  $\delta^{18}O$  values which are biased towards brine composition, the temperatures given by this model varied depending on brine emplacement and are displayed separately in Fig. 10a.

# 4. DISCUSSION

# 4.1. Synthetic carbonate calibration for clumped isotopes

The relationship between temperature and  $\Delta_{47}$  values in the precipitated carbonates produces a statistically similar regression to those derived by previous workers (Dennis and Schrag, 2010; Passey and Henkes, 2012; Tang et al., 2014; Kluge et al., 2015; Kelson et al., 2017), as is shown in Fig. 5. Of these, only Kelson et al. (2017) was calculated using the Brand parameters for PDB and  $\lambda$  (Daëron et al., 2016). The Pearson's coefficient for the temperature- $\Delta_{47}$ relationship of the residuals of all synthetic carbonate values from this study and Kelson et al.'s calibration is -0.19 (p = 0.25). When an acid fractionation factor of +0.092 (Passey et al., 2010) is applied to Kelson's calibration, the two calibrations are comparable (Fig. 5). Because the measurements of  $\Delta_{47}$  values on the synthetic carbonate samples in this study were measured using an identical procedure to that employed for the natural materials, all paleotemperature estimates in this study will use Eq. (4). This

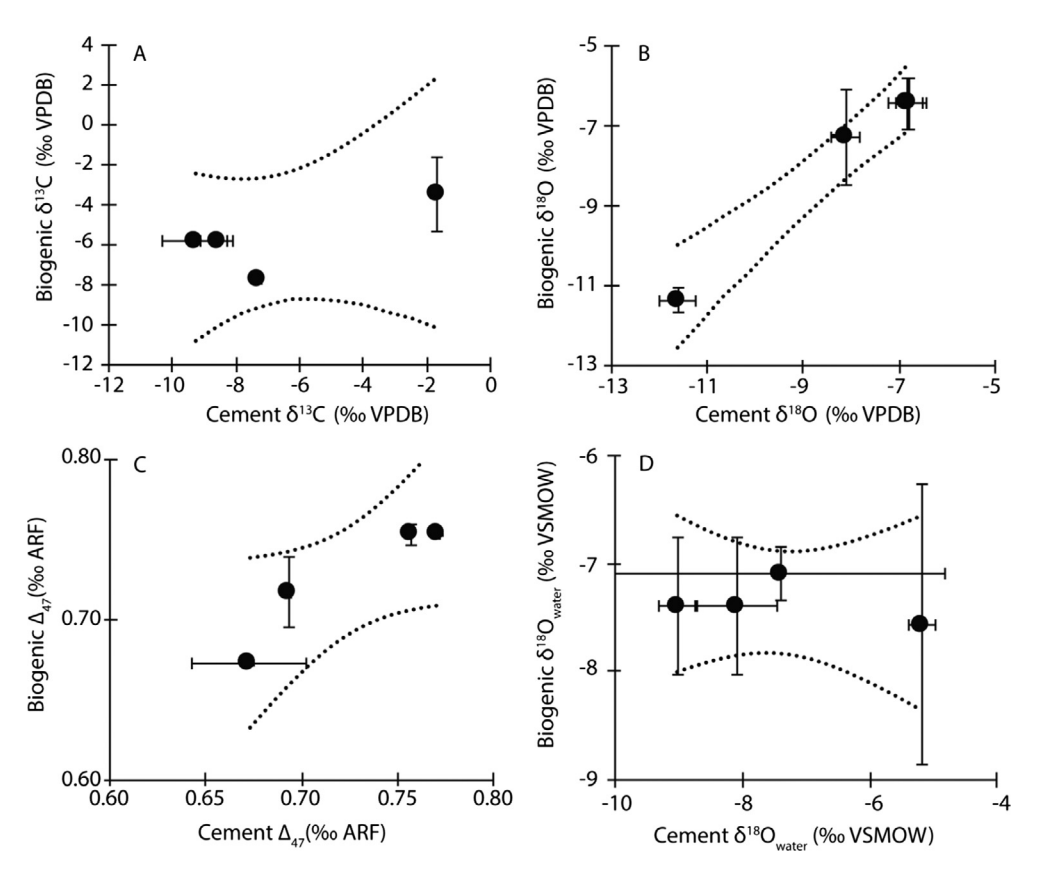


Fig. 9. (A) Covariance between cement and biogenic  $\delta^{13}$ C values (p = 0.286). (B) Covariance between cement and biogenic  $\delta^{18}$ O values (p = 0.006). (C) Covariance between cement and biogenic  $\delta^{18}$ O<sub>water</sub> values (p = 0.018).

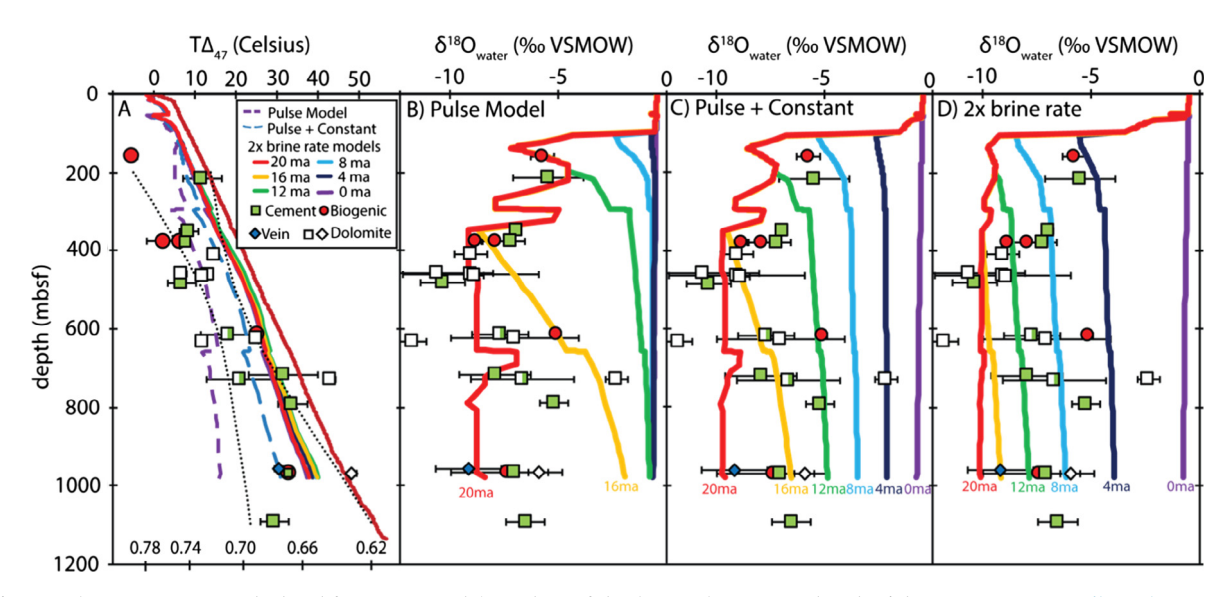


Fig. 10. (A) Temperatures calculated from measured  $\Delta_{47}$  values of the AND-2A Core, modern burial temperatures (Wonik et al., 2008) and  $\Delta_{47}$  output from "Pulse", "Pulse + Constant" and "2x Brine Rate" models. (B)  $\delta^{18}O_{water}$  values calculated using clumped isotopes and  $\delta^{18}O_{mater}$  measurements of the AND-2A Core and the  $\delta^{18}O_{water}$  output of the "Pulse" rate model different color lines reflect output of different modeled times of brine emplacement. (C)  $\delta^{18}O_{water}$  values calculated using clumped isotopes and  $\delta^{18}O$  measurements of the AND-2A Core and the  $\delta^{18}O_{water}$  output of the "Pulse + Constant" rate model. (D)  $\delta^{18}O_{water}$  values calculated using clumped isotopes and  $\delta^{18}O$  measurements of carbonates from the AND-2A Core and the output of  $\delta^{18}O_{water}$  values from the "2x brine rate" rate model. Displayed model results in B, C and D are the output of 6 model runs, which simulate brine infiltration time in 4 Myr increments.

eliminates any potential for inter-laboratory differences in preparation technique and data processing.

The calculated  $\alpha_{water-carbonate}$  values for each temperature are slightly more positive than those commonly obtained from the Kim and O'Neil (1997) relationship (Fig. 6), which was precipitated at 5 mM DIC concentration. In the same study, another calibration was produced at 25 mM DIC, which is more positive than ours. Subsequent determination of fluid  $\delta^{18}$ O values using clumped isotopes in this study will nevertheless use the commonly used relationship from Kim and O'Neil (1997).

#### 4.2. Cement carbonate composition for AND-2A

The  $\delta^{13}$ C values of the calcite and dolomite cements varied, suggesting that they may have formed by different mechanisms. This variability in  $\delta^{13}$ C values is consistent with the observed differences in the composition of dissolved inorganic carbonate (DIC) in the pore fluids (Fig. 7a). The highly variable  $\delta^{13}$ C values in calcite suggest multiple sources of carbon, with extremely negative values possibly derived from the oxidation of methane and more positive values derived from a mixture of respired organic material and seawater carbonate (Fig. 8). The narrower range and more positive  $\delta^{13}$ C values found in the dolomites suggests that carbon sources with more negative  $\delta^{13}$ C values did not contribute to their formation. Subsequent recrystallization of these cements potentially in the brine, could preserve their  $\delta^{13}$ C values if the fraction of carbon in the cements exceeds the available DIC reservoir. The  $\delta^{18}$ O values would not be expected to display this buffering, as there is considerably more oxygen in the porewater than in the carbonate cement.

One calcitic sample (223.20 mbsf) possessed an extremely negative  $\delta^{13}$ C value of -28% and yielded an anomalously warm temperature estimate of  $37.4 \pm 4.4$  °C and a resultant  $\delta^{18}$ O value of  $\pm 2.6 \pm 0.7\%$ . The  $\Delta_{48}$  value of this sample is within 1 standard deviation of the mean value obtained from other samples, suggesting that this high temperature was not due to sample contamination. This sample contained less than 5% carbonate cement and thus would be extremely susceptible to contamination from minor carbonate sources. Petrographic analysis of the anomalous sample also shows trace amounts of detrital marble (Fig. 2a), which may have contaminated this sample with high-temperature metamorphic carbonate from a metamorphic province on the continent (Huntington and Lechler, 2015). Analyses of clasts in the AND-2A core suggest that detrital grains at this depth are likely sourced from ice sheets that did not extend far from the coastal margin, and thus represent a fairly local population (Cornamusini and Talarico, 2016). Isotopic analysis of 21 local metamorphic carbonates in the Victoria Land region yielded far more positive  $\delta^{13}$ C values ranging between 3.6 and -2.5% (Worley et al., 1995), this possibly necessitates some other source for these isotopically negative carbonate  $\delta^{13}$ C values. It is possible that the anomalous temperature could be a result of non-linear  $\Delta_{47}$  mixing of sediments of different isotopic composition (Defliese and Lohmann, 2015), a negative mixing for  $\Delta_{47}$  values requires mixing of two endmembers with negatively correlated  $\delta^{13}C$  and  $\delta^{18}O$  values. Producing an offset in  $\Delta_{47}$  value of -0.15%, necessary to produce this discrepant temperature, would require an offset of 40% between these end members. This would require a source of carbon with negative  $\delta^{13}C$  values, -70%. Methane oxidation by bacterial sulfate reduction (BSR) is another possible candidate as it has the potential to produce carbonate materials with negative  $\delta^{13}C$  values that are out of equilibrium with respect to temperatures calculated using  $\Delta_{47}$  values due to kinetic effects by as much as -0.2%, resulting in significantly warmer calculated temperatures (Loyd et al., 2016). We consider BSR to be the most likely cause of the disequilibrated  $\Delta_{47}$  value for this sample. The outlying  $T\Delta_{47}$  value is omitted from statistics, but is nonetheless plotted in Fig. 7, labeled BSR Calcite.

The  $\Delta_{47}$  values of the diagenetic and biogenic carbonates decrease with increasing depth, indicating formation of carbonate minerals and recrystallization at increasingly higher temperatures (Fig. 7c). Linear interpolation of temperatures derived from  $\Delta_{47}$  values indicate a downcore temperature gradient of  $42.8 \pm 7.9$  °C/km ( $r^2 = 0.66$ , n = 17). This slope is parallel to the present geothermal gradient as described by Wonik et al. (2008) (43.9 °C/km between 200 and 1200 mbsf) (p = 0.88, where  $r^2 = 0.017$  for residual). Temperatures calculated from  $\Delta_{47}$  values are offset towards cooler temperatures than current burial values, offset by  $11.5 \pm 7.0$  °C (Fig. 7c). Because each individual analysis potentially integrates a range of cementation temperatures during burial; it is expected that cooler temperatures from earlier burial would be recorded in the cements' isotopic compositions. Translating the modern burial depths upward such that the geothermal gradient predicted using  $\Delta_{47}$  values equals the modern geothermal gradient indicates an average depth of cementation  $260 \pm 100 \,\mathrm{m}$  shallower than current burial depth. This depth includes a series of depositional hiatuses during the Miocene described by Acton et al. (2008) and Levy et al. (2016). A substantial fraction of the cementation could have taken place during these prolonged periods of minimal sediment accumulation (3-11 Ma) when the geothermal gradient would have remained relatively constant. This offset in temperature could also be partially the result of cooler initial temperatures, although the relatively consistent downcore reconstructed  $T\Delta_{47}$  of bivalves measured by Levy et al. (2016) seem to preclude this interpretation.

Although the  $\delta^{18}O_{water}$  values derived from  $\Delta_{47}$  and  $\delta^{18}O_{carbonate}$  values exhibit some variability, they occupy a similar range to observed brine  $\delta^{18}O_{water}$  values. These observations are consistent with cements forming predominantly in the presence of the cryogenic brine, with the  $\Delta_{47}$  values recording the temperatures of cements forming over the burial history. The  $\delta^{18}O$  values in DIC equilibrate more slowly at cooler temperatures (Beck et al., 2005), extrapolation of equilibration rates measured between 15–40 °C and 0 °C estimates an equilibration rate with a half-life of approximately 40 h. Our interpretations rely on the assumption that the diagenetic processes occurred at a sufficiently slow rate that DIC had sufficient time to equilibrate during the precipitation of carbonate cements. It has been observed in some settings that rapid precipitation

of carbonate minerals, such as those described earlier in the presence of BSR, can occur sufficiently rapidly to be out of equilibrium (Loyd et al., 2016). We argue that the conditions of deeper burial are closer to chemical and isotopic equilibrium with residence times of DIC far exceeding the requisite time for complete equilibration.

Isotopic analyses of the nearby AND-1B core showed similarly negative  $\delta^{18}O$  values in carbonates, as low as -13% (Pompilio et al., 2007). These values did not show a downcore trend from more positive to more negative values as is shown in Fig. 7b. It is therefore likely that these two sites'  $\delta^{18}O$  values are influenced by very different processes.

If a significant fraction of cement formed at a depth corresponding to the hiatuses between 3 and 11 Ma, with some cement having formed before and after this interval, then a diagenetic fluid isotopically similar to the cryogenic brine must have been present in the subsurface of the VLB since at least the Late Miocene. A mixture of primary and diagenetic carbonate minerals could also account for this trend in crystallization temperatures, but would necessitate a covariance between temperature and the calculated  $\delta^{18}$ -Owater values, trending from the isotopic composition of seawater to that of the brines described by Frank et al. (2010); this has not been observed in cements. Even the most deeply buried carbonates, with  $\Delta_{47}$  temperatures that deviate the most from the temperatures measured during logging, still record brine  $\delta^{18}O_{water}$  values within the range and uncertainty of overlying cement values.

Using the methods described herein, calcite and dolomite yield essentially the same  $T\Delta_{47}$  and  $\delta^{18}O_{water}$  values and display no significant downcore trends in calculated fluid  $\delta^{18}$ O values with depth (Fig. 7c and d). If the dolomite-specific temperature calibration with no difference in acid fractionation factor, proposed by Bonifacie et al. (2017) is applied to dolomite at this site, a consistently higher temperature, and thus more enriched reconstructed fluid  $\delta^{18}$ O values are determined. These reconstructed dolomite temperatures are on average 10 °C warmer than present burial temperatures, which is implausible considering the burial history of the site. A revised version of Fig. 7 using the Bonifacie et al. (2017) paleotemperature equation is available in the supplemental material. The use of the Murray et al. (2016) methodology results in dolomite and calcite cements yielding similar cementation temperatures and fluid compositions.

#### 4.3. Biogenic carbonate

In this study, five biogenic materials were analyzed, four of which were accompanied by an analysis of the adjacent matrix. Biogenic carbonate records cooler temperatures at 377.54 mbsf, warmer at 616.36 mbsf, and virtually identical (968.53 mbsf) values than the corresponding sediment matrix. Biogenic carbonates reconstruct fluid  $\delta^{18}$ O values ranging between -5.2 and -8.9% relative to VSMOW. It is not impossible that the initial fluids forming the biogenic materials may have been isotopically negative due to mixing with glacial meltwater. However, the temperatures reconstructed using  $\Delta_{47}$  values suggests that apart from the bar-

nacle shell, all have recrystallized deeper in the geothermal gradient and in the presence fluid with brine-like  $\delta^{18}O$  values. The bivalves described here were likely initially aragonite, which was subsequently neomorphosed to calcite. Serpulid worm tubes may vary in mineralogy (Vinn et al., 2008) and thus the initial mineralogy of the tube at 337.54 mbsf is unknown, the current mineralogy however, is 100% calcite. The difference in isotopic composition between cements and secondary calcite in the shell molds suggest that cementation and neomorphism occurred at separate times and the temperatures from  $\Delta_{47}$  values indicate that there is no consistent time or depth where the secondary calcite forms.

The barnacle, sampled at 158.80 mbsf, had a  $\delta^{18}O_{carbonate}$  value of -2.9% and an interpreted formation temperature of  $-5.0 \pm 1.3$  °C, although this value is extrapolated from the inorganic calibration range presented in this study. Together, these two values result in a calculated fluid  $\delta^{18}O$  value of  $-5.9 \pm 0.5\%$  VSMOW. Modern barnacles tend to form carbonates with slightly more positive  $\delta^{18}O$  values with respect to equilibrium calcite (Killingley and Newman, 1982), isotope analyses of barnacles in the Ross Sea have a typical range from +4 to +5% VPDB, forming at -2°C (Burgess et al., 2010).

Analyses of unaltered biogenic carbonates by Levy et al. (2016) yielded isotopic compositions significantly offset from those presented in this study (Figs. 7 + 8, solid black dots), giving nearly vertical downcore trends for all measured values, with values similar to modern carbonates in the Ross Sea area. The  $T\Delta_{47}$  values for the more deeply buried biogenic materials described in this study are higher than the unaltered material described in Levy et al. (2016) below 600 mbsf, although these recrystallized bivalves are not at equilibrium with modern burial temperatures (Fig. 7c).

Reconstructed water  $\delta^{18}O$  and carbonate  $\delta^{13}C$  values fall along a linear continuum trending from the unaltered carbonates described by Levy et al. (2016) to a point within the range of modern pore fluid compositions (Fig. 8). This linear trend is not observed in  $T\Delta_{47}$  temperatures, likely indicating that this trend is due to recrystallization in a fluid of distinct isotopic composition (e.g. the brine), however, this recrystallization did not occur at a single depth or temperature.

## 4.4. Vein carbonate

The two vein carbonates sampled in this study are mineralogically and isotopically distinct from one another. The dolomite vein at 968.96 mbsf records warmer burial temperatures, consistent with those observed in cements in the overlying sediments, suggesting it formed during the same period. By contrast, the calcite vein fill at 958.70 mbsf records cooler burial temperatures and more negative carbon isotope values, suggesting it may have formed at a shallower depth, and thus at an earlier time. If it is assumed that the fracture infills formed as single events, it is possible to calculate the depth, and thus time, at which cementation occurred using the  $T\Delta_{47}$  values and assuming a constant geothermal gradient. The shallower fracture formed at 30

 $\pm$  7 °C, and is buried where the ambient temperature is 46 ° C (Wonik et al., 2008). Using the local geothermal gradient of 43 °C/km, disequilibrium suggests infill occurred approximately  $370 \pm 160 \,\mathrm{m}$  shallower than its modern burial depth, indicating that this vein formed between 11 and 16 Ma. Clumped isotope analyses of the more deeply buried dolomite infill indicate a formation temperature of 48  $\pm$  2  $^{\circ}$ C, this vein is presently buried at 47 °C, suggesting a far more recent time of formation, as the sample is within uncertainty of its present burial temperature. Migrating hydrothermal fluids may also have played a role at this site, in which case these interpretations would overestimate burial depth. Calculating fluid composition using the  $T\Delta_{47}$  values and the measured carbonate  $\delta^{18}$ O values indicates that both veins formed in the presence of a fluid with  $\delta^{18}O$  value between -6 and -9% relative to SMOW, consistent with the present-day measurements at the site.

# 4.5. Comparison between measured and modeled results

Analyses of cements, veins, and neomorphosed biogenic carbonates indicate that a significant amount of carbonate formed at cooler temperatures than modern burial depths and in the presence of a fluid with brine-like  $\delta^{18}O$  values. Models show that this can be accomplished in two ways: increased duration of exposure to brines, or through increased rates of cementation in the presence of the brine. Using  $\delta^{18}O_{carbonate}$  values alone, it is impossible to differentiate these two scenarios. Clumped isotopes are sensitive only to temperature, and therefore burial depth, and thus can determine the average depth of cementation (Fig. 10a).

The "pulse" model yields the lowest  $T\Delta_{47}$  values for cements, because it is the most offset towards early diagenetic temperatures and the warmest temperatures are output by the "2x Brine Rate" model. Together, these two models provide upper and lower brackets for the measured  $T\Delta_{47}$  values in cements. These differences clearly show the effect cementation rates and depths can have on the resulting composition, suggesting that adjacent sediment units can have dramatically different compositions even if they are subjected to identical burial rates and brine emplacement times.

Measured  $\delta^{18}O_{water}$  values from  $\Delta_{47}$  values in cements range between -6% and -11% (SMOW), which is ostensibly the range predicted from all models. Different rates of recrystallization, however, suggest different times of brine emplacement. Because of uncertainties within the measured data, it is difficult to determine a definitive time of brine infiltration. It is, however, possible to conclude that the brine has been present for significant periods of time. The "Pulse + Constant" and "2x Brine rate" models both predict temperatures that reasonably describe more deeply buried cements, and are biased towards earlier times of brine emplacement. Based on these two models, brines are not likely to have infiltrated later than 8 Ma, and were likely to have been present even earlier.

Because each measured sample value is a result of the integrated chemistry over its entire depositional history, which can vary greatly between different sedimentary units (Dunham et al., 2017), no single diagenetic rate model can

completely describe the entire sediment column. Nevertheless, these models predict that a fluid with brine-like  $\delta^{18}O$  values has been present for a substantial period of time, the most conservative estimate being at least 8 Ma. The nature of these models and analyses preclude a definitive maximum estimate. Nevertheless, the most deeply buried sediments, whose calculated temperatures are the most skewed towards cooler, earlier diagenetic temperatures, appear to be best described by the "Pulse + Constant" model, suggesting fluids with brine  $\delta^{18}O$  values have been present in the Victoria Land Basin as early as 12–16 Ma, coincident with the onset of permanent glaciation in the region and are consistent with the cryogenic interpretation of their origin by Frank et al. (2010).

# 4.6. Implications for the interpretation of glaciomarine deposits

Cryogenic brines, such as those described at AND-2A, are presently formed at high latitudes and can be produced in numerous coastal environments (e.g. flexural troughs in Fig. 4a and semi-isolated coastal lakes in Fig. 4b). It seems therefore likely that during other periods of Earth's history, for instance during the late Paleozoic ice ages (Fielding et al., 2008b) when polar temperatures were periodically cold enough to freeze seawater, similar brines could have been produced. The apparently long-lived brines discussed in this manuscript suggest that this has been the case in the Victoria Land Basin since as early as the mid Miocene. This is likewise true for sediments during Neoproterozoic "snowball earth" events (Hoffman and Schrag, 2002), where ice-proximal coastal basins could have experienced a similar early diagenetic history to the sediments in the VLB. Calcite and dolomite cements as well as other secondary carbonates are likely to record the negative  $\delta^{18}$ O values of these brines, as has been demonstrated in this study. The  $\delta^{13}$ C values and reconstructed  $\delta^{18}$ O<sub>water</sub> values from carbonates are within the range between porewater and unaltered biogenic carbonates (Fig. 8), incorporating the lighter isotopic compositions imparted by the modern cryogenic brine. Interpretation of analogous authigenic carbonates with these isotopic compositions may implicate a meteoric source of water, however cryogenic brines provide an additional mechanism for producing cements and secondary minerals with these compositions. It is possible that these cements could provide clues of seawater freezing and brine formation which otherwise may leave little sedimentary evidence behind.

#### 5. CONCLUSIONS

The  $T\Delta_{47}$  values derived from the cements and recrystal-lized biogenic carbonates indicate that the bulk of diagenetic chemistry occurred at slightly cooler temperatures than those in the present geothermal gradient, indicative of cementation during earlier stages of burial. This bias towards cooler temperatures indicates an average depth of cementation 260 mbsf above the present burial depth, which coincides with a slowing in sediment accumulation rate. Recrystallized biogenic carbonates and vein carbon-

ates incorporate this negative  $\delta^{18}O_{water}$  value, and record warmer  $T\Delta_{47}$  values and more negative fluid  $\delta^{18}$ O values than the unaltered biogenic carbonates described by Levy et al. (2016). Using variable cementation rates, time integrated models output the range in measured  $T\Delta_{47}$  values of cements, and suggest that a fluid with the isotopic composition of the brines was likely present after the Miocene Climatic Optimum (16 Ma), during which the region transitioned to its present cold, polar state. These brines provide a mechanism for producing isotopically depleted carbonate materials without the need for invoking high-temperature or meteoric alteration. The capacity for brine formation exists in many coastal high-latitude settings; therefore, it is likely that fluids such as these have played a role not only in the VLB, but other ice-proximal sediments and basins throughout the geologic record.

#### ACKNOWLEDGEMENTS

This research was made possible through the ANDRILL SMS Team's efforts, as well as funding through PRF Grant #AC-52863ND2 and NSF Grant #PLR-1341390 to TDF and CRF. The manuscript benefited from the editing of Greta Mackenzie. Chris Kaiser is acknowledged for his technical support with XRD. Acquisition of the Thermo-253 was funded under NSF grant EAR0926503 to PKS. We are grateful to the editors of GCA and three anonymous reviewers whose suggestions and critiques improved this manuscript.

# APPENDIX A. SUPPLEMENTARY MATERIAL

Individual isotopic measurements for synthetic carbonates and natural materials described in this study are available as supplementary tables. Supplementary data associated with this article can be found, in the online version, at https://doi.org/10.1016/j.gca.2018.01.002.

# REFERENCES

- Acton G., Crampton J., Vincenzo G. D., Fielding C. R. and Florindo F. (2008) Preliminary integrated chronostratigraphy of the AND-2A core. *ANDRILL Southern McMurdo Sound Project, Antarctica: Terra Antarctica* **15**(1), 211–220.
- Allan J. and Matthews R. (1982) Isotope signatures associated with early meteoric diagenesis. *Sedimentology* **29**(6), 797–817.
- Assonov S. S. and Brenninkmeijer C. A. (2003) A redetermination of absolute values for 17RVPDB-CO2 and 17RVSMOW. *Rapid Commun. Mass Spectrom.* 17(10), 1017–1029.
- Baertschi P. (1976) Absolute <sup>18</sup>O content of standard mean ocean water. *Earth Planet. Sci. Lett.* **31**(3), 341–344.
- Barkan E. and Luz B. (2005) High precision measurements of <sup>17</sup>O/<sup>16</sup>O and <sup>18</sup>O/<sup>16</sup>O ratios in H<sub>2</sub>O. *Rapid Commun. Mass Spectrom.* **19**(24), 3737–3742.
- Barker P. F., Diekmann B. and Escutia C. (2007) Onset of Cenozoic Antarctic glaciation. *Deep Sea Res. Part II* 54(21–22), 2293–2307.
- Beck W. C., Grossman E. L. and Morse J. W. (2005) Experimental studies of oxygen isotope fractionation in the carbonic acid system at 15, 25, and 40 C. *Geochim. Cosmochim. Acta* 69(14), 3493–3503.
- Beu A., Taviani M. and Sigwart J. (2014) Early Miocene mollusca from McMurdo Sound, Antarctica (ANDRILL 2A drill core),

- with a review of Antarctic Oligocene and Neogene Pectinidae (Bivalvia). *Palaeontology* **57**(2), 299–342.
- Black R. F. and Bowser C. J. (1967) Salts and associated phenomena of the termini of the Hobbs and Taylor Glaciers, Victoria Land, Antarctica. Gen. Assembly Gern. 25, 226–238.
- Bonifacie M., Calmels D., Eiler J. M., Horita J., Chaduteau C., Vasconcelos C., Agrinier P., Katz A., Passey B. H., Ferry J. M. and Bourrand J.-J. (2017) Calibration of the dolomite clumped isotope thermometer from 25 to 350 °C, and implications for a universal calibration for all (Ca, Mg, Fe)CO<sub>3</sub> carbonates. *Geochim. Cosmochim. Acta* 200, 255–279.
- Bottomley D. J., Renaud R., Kotzer T. and Clark I. D. (2002) Iodine-129 constraints on residence times of deep marine brines in the Canadian Shield. *Geology* 30(7), 587–590.
- Bottomley D. J., Clark I. D., Battye N. and Kotzer T. (2005) Geochemical and isotopic evidence for a genetic link between Canadian Shield brines, dolomitization in the Western Canada Sedimentary Basin, and Devonian calcium-chloridic seawater. Can. J. Earth Sci. 42(11), 2059–2071.
- Bowser C., Rafter T. and Black R. (1970) Geochemical evidence for the origin of mirabilite deposits near Hobbs Glacier, Victoria Land, Antarctica: Mineral. Soc. Am. Spec. Pap. 3, 261–272
- Brady H. T. and Batts B. (1981) Large salt beds on the surface of the Ross Ice Shelf near Black Island, Antarctica. *J. Glaciol.* **27** (95), 11–18.
- Brand W. A., Assonov S. S. and Coplen T. B. (2010) Correction for the 17O interference in δ(13C) measurements when analyzing CO2 with stable isotope mass spectrometry (IUPAC Technical Report): Pure and Applied Chemistry, v. 82, no. 8.
- Burgess S. N., Henderson G. M. and Hall B. L. (2010) Reconstructing Holocene conditions under the McMurdo Ice Shelf using Antarctic barnacle shells. *Earth Planet. Sci. Lett.* 298(3–4), 385–393.
- Burns S. J. and Matter A. (1995) Geochemistry of carbonate cements in surficial alluvial conglomerates and their paleoclimatic implications, Sultanate of Oman. J. Sediment. Res. 65(1).
- Butler B. M., Papadimitriou S., Santoro A. and Kennedy H. (2016) Mirabilite solubility in equilibrium sea ice brines. *Geochim. Cosmochim. Acta* 182, 40–54.
- Cartwright J. H., Escribano B., Gonzalez D. L., Sainz-Diaz C. I. and Tuval I. (2013) Brinicles as a case of inverse chemical gardens. *Langmuir* 29(25), 7655–7660.
- Chang T. and Li W. (1990) A calibrated measurement of the atomic-weight of carbon. Chin. Sci. Bull. 35(4), 290–296.
- Cornamusini G. and Talarico F. M. (2016) Miocene Antarctic ice dynamics in the Ross Embayment (Western Ross Sea, Antarctica): insights from provenance analyses of sedimentary clasts in the AND-2A drill core. *Global Planet. Change* **146**, 38–52.
- Coxall H. K., Wilson P. A., Palike H., Lear C. H. and Backman J. (2005) Rapid stepwise onset of Antarctic glaciation and deeper calcite compensation in the Pacific Ocean. *Nature* 433(7021), 53.
- Daëron M., Blamart D., Peral M. and Affek H. P. (2016) Absolute isotopic abundance ratios and the accuracy of  $\Delta_{47}$  measurements. *Chem. Geol.* **442**, 83–96.
- Dayton P. K. and Martin S. (1971) Observations of ice stalactites in McMurdo Sound, Antarctica. J. Geophys. Res. 76(6), 1595– 1599
- Defliese W. F., Hren M. T. and Lohmann K. C. (2015) Compositional and temperature effects of phosphoric acid fractionation on Δ47 analysis and implications for discrepant calibrations. *Chem. Geol.* **396**, 51–60.
- Defliese W. F. and Lohmann K. C. (2015) Non-linear mixing effects on mass-47 CO<sub>2</sub> clumped isotope thermometry: patterns and implications. *Rapid Commun. Mass Spectrom.* **29**(9), 901–909

- Dennis K. J. and Schrag D. P. (2010) Clumped isotope thermometry of carbonatites as an indicator of diagenetic alteration. *Geochim. Cosmochim. Acta* **74**(14), 4110–4122.
- Dennis K. J., Affek H. P., Passey B. H., Schrag D. P. and Eiler J. M. (2011) Defining an absolute reference frame for 'clumped' isotope studies of CO<sub>2</sub>. *Geochim. Cosmochim. Acta* 75(22), 7117–7131.
- Dunham D. P., Frank T. D. and Fielding C. R. (2017) Climate, sea level, and reservoir quality in deposits of polar glacimarine settings: insights from the neogene succession of the Victoria Land Basin. SEPM Special Publication, Antarctica, p. 108.
- Eiler J. M. (2011) Paleoclimate reconstruction using carbonate clumped isotope thermometry. *Quat. Sci. Rev.* 30(25–26), 3575– 3588
- Engel A., Clayton R. and Epstein S. (1958) Variations in isotopic composition of oxygen and carbon in Leadville limestone (Mississippian, Colorado) and in its hydrothermal and metamorphic phases. *J. Geol.* **66**(4), 374–393.
- Fernandez A., Müller I. A., Rodríguez-Sanz L., van Dijk J., Looser N. and Bernasconi S. M. (2017) A reassessment of the precision of carbonate clumped isotope measurements: implications for calibrations and paleoclimate reconstructions. Geochem., Geophys., Geosyst.
- Fielding C. R., Atkins C. B., Bassett K. N., Browne G. H., Dunbar G. B., Field B. D., Frank T. D., Krissek L. A., Panter K. S., Passchier S., Pekar S. F., Sandroni S., Talarico F. and Team A.-S. S. (2008a) Sedimentology and stratigraphy of the AND-2A core, ANDRILL Southern McMurdo sound project, Antarctica. *Terra Antarctica* 15(1), 77–122.
- Fielding C. R., Frank T. D. and Isbell J. L. (2008b) The late Paleozoic ice age—a review of current understanding and synthesis of global climate patterns 441, 343–354.
- Fielding C. R., Browne G. H., Field B., Florindo F., Harwood D. M., Krissek L. A., Levy R. H., Panter K. S., Passchier S. and Pekar S. F. (2011) Sequence stratigraphy of the ANDRILL AND-2A drillcore, Antarctica: a long-term, ice-proximal record of Early to Mid-Miocene climate, sea-level and glacial dynamism. *Palaeogeogr., Palaeoclimatol., Palaeoecol.* 305(1–4), 337–351.
- Fielding C. R., Blackstone B. A., Frank T. D. and Gui Z. (2012) Reservoir potential of sands formed in glaciomarine environments: an analogue study based on Cenozoic examples from McMurdo Sound, Antarctica. *Geol.Soc.*, *London*, *Special Publications* 368(1), 211–228.
- Frank T. D., Gui Z. and Team A. S. S. (2010) Cryogenic origin for brine in the subsurface of southern McMurdo Sound, Antarctica. *Geology* **38**(7), 587–590.
- Galeotti S., DeConto R., Naish T., Stocchi P., Florindo F., Pagani M., Barrett P., Bohaty S. M., Lanci L. and Pollard D. (2016) Antarctic Ice Sheet variability across the Eocene-Oligocene boundary climate transition. *Science* 352(6281), 76–80.
- Garrett D. E. (2001) Sodium Sulfate: Handbook of Deposits, Processing, & Use. Academic press.
- Ghosh P., Adkins J., Affek H., Balta B., Guo W., Schauble E. A., Schrag D. and Eiler J. M. (2006) <sup>13</sup>C–<sup>18</sup>O bonds in carbonate minerals: a new kind of paleothermometer. *Geochim. Cos-mochim. Acta* 70(6), 1439–1456.
- Grasby S. E., Smith I. R., Bell T. and Forbes D. L. (2013) Cryogenic formation of brine and sedimentary mirabilite in submergent coastal lake basins, Canadian Arctic. *Geochim. Cosmochim. Acta* 110, 13–28.
- Grossman E. L. and Ku T.-L. (1986) Oxygen and carbon isotope fractionation in biogenic aragonite: temperature effects. *Chem. Geol.* **59**, 59–74.
- He B., Olack G. A. and Colman A. S. (2012) Pressure baseline correction and high-precision CO<sub>2</sub> clumped-isotope (Δ47)

- measurements in bellows and micro-volume modes. *Rapid Commun. Mass Spectrom.* **26**(24), 2837–2853.
- Herrero M. J., Escavy J. I. and Schreiber B. C. (2015) Thenardite after mirabilite deposits as a cool climate indicator in the geological record: lower Miocene of central Spain. *Clim. Past* 11(1), 1–13.
- Herut B., Starinsky A., Katz A. and Bein A. (1990) The role of seawater freezing in the formation of subsurface brines. *Geochim. Cosmochim. Acta* **54**(1), 13–21.
- Hoffman P. F. and Schrag D. P. (2002) The snowball Earth hypothesis: testing the limits of global change. *Terra Nova* **14** (3), 129–155.
- Horita J. (2008) Isotopic evolution of saline lakes in the low-latitude and polar regions. *Aquat. Geochem.* **15**(1–2), 43–69.
- Huntington K. W., Budd D. A., Wernicke B. P. and Eiler J. M. (2011) Use of clumped-isotope thermometry to constrain the crystallization temperature of diagenetic calcite. *J. Sediment. Res.* **81**(9), 656–669.
- Huntington K. W. and Lechler A. R. (2015) Carbonate clumped isotope thermometry in continental tectonics. *Tectonophysics* **647–648**, 1–20.
- Kelson J. R., Huntington K. W., Schauer A. J., Saenger C. and Lechler A. R. (2017) Toward a universal carbonate clumped isotope calibration: diverse synthesis and preparatory methods suggest a single temperature relationship. *Geochim. Cosmochim. Acta* 197, 104–131.
- Kennett J. P. (1977) Cenozoic evolution of Antarctic glaciation, the circum-Antarctic Ocean, and their impact on global paleoceanography. J. Geophys. Res. 82(27), 3843–3860.
- Killingley J. and Newman W. (1982) O<sup>18</sup> fractionation in barnacle calcite: a barnacle paleotemperature equation. *J. Mar. Res.* **40** (3), 893–902.
- Kim S.-T. and O'Neil J. R. (1997) Equilibrium and nonequilibrium oxygen isotope effects in synthetic carbonates. *Geochim. Cosmochim. Acta* 16, 3461–3475.
- Kim S.-T., O'Neil J. R., Hillaire-Marcel C. and Mucci A. (2007) Oxygen isotope fractionation between synthetic aragonite and water: influence of temperature and Mg<sup>2+</sup> concentration. *Geochim. Cosmochim. Acta* 71(19), 4704–4715.
- Kluge T., John C. M., Jourdan A.-L., Davis S. and Crawshaw J. (2015) Laboratory calibration of the calcium carbonate clumped isotope thermometer in the 25–250 °C temperature range. *Geochim. Cosmochim. Acta* **157**, 213–227.
- Lambert S. J. and Carter J. A. (1984) Uranium-isotope disequilibrium in brine reservoirs of the castile formation, Northern Delaware Basin, Souteastern New Mexico I: principles and methods. Sandia National Laboratories, SAND83-0144.
- Land L. S. and Epstein S. (1970) Late Pleistocene diagenesis and dolomitization, north Jamaica. Sedimentology 14(3-4), 187– 200.
- Levy R., Harwood D., Florindo F., Sangiorgi F., Tripati R., von Eynatten H., Gasson E., Kuhn G., Tripati A., DeConto R., Fielding C., Field B., Golledge N., McKay R., Naish T., Olney M., Pollard D., Schouten S., Talarico F., Warny S., Willmott V., Acton G., Panter K., Paulsen T., Taviani M. and Team S. M. S. S. (2016) Antarctic ice sheet sensitivity to atmospheric CO<sub>2</sub> variations in the early to mid-Miocene. *Proc. Natl. Acad. Sci. USA* 113(13), 3453–3458.
- Louvat D., Michelot J. L. and Aranyossy J. F. (1999) Origin and residence time of salinity in the Äspö groundwater system. *Appl. Geochem.* **14**, 917–925.
- Loyd S. J., Sample J., Tripati R. E., Defliese W. F., Brooks K., Hovland M., Torres M., Marlow J., Hancock L. G., Martin R., Lyons T., Tripati A. E. (2016) Methane seep carbonates yield clumped isotope signatures out of equilibrium with formation temperatures. Nat. Commun. 7, 12274.

- Marcano M. C., Frank T. D., Mukasa S. B., Lohmann K. C. and Taviani M. (2015) Diagenetic incorporation of Sr into aragonitic bivalve shells: implications for chronostratigraphic and palaeoenvironmental interpretations. *Depositional Rec.* 1(1), 38–52.
- Matthews A. and Katz A. (1977) Oxygen isotope fractionation during the dolomitization of calcium carbonate. *Geochim. Cosmochim. Acta* 41(10), 1431–1438.
- Millan C. (2013) Syntectonic fluid flux in a glaciated rift basin: record from vein arrays in the AND-1B and AND-2A sedimentary rock cores, Victoria Land Basin, Antarctica [Ph. D.: Ohio State University, 246 p.
- Müller I. A., Violay M. E., Storck J.-C., Fernandez A., Van Dijk J., Madonna C. and Bernasconi S. M. (2017) Clumped isotope fractionation during phosphoric acid digestion of carbonates at 70 °C. *Chem. Geol.* **449**, 1–14.
- Murray S. (2016) The application of clumped isotopes in the study of dolomitization. PhD: UNiversity of Miami, 213 p.
- Murray S. T., Arienzo M. M. and Swart P. K. (2016) Determining the  $\Delta_{47}$  acid fractionation in dolomites. *Geochim. Cosmochim. Acta* 174, 42–53.
- Murray S. T. and Swart P. K. (2017) Evaluating formation fluid models and calibrations using clumped isotope paleothermometry on Bahamian dolomites. *Geochim. Cosmochim. Acta* **206**, 73\_93
- Nelson K. H. and Thompson T. G. (1954) Deposition of salts from sea water by frigid concentration. *J. Mar. Res.* 13, 166–182.
- Paige R. A. (1970) Stalactite growth beneath sea ice. *Science* **167** (3915), 171–172.
- Panter K., Talarico F., Bassett K., Del Carlo P., Field B., Frank T., Hoffmann S., Kuhn G., Reichelt L. and Sandroni S. (2008) Petrologic and Geochemical Composition of the AND-2A Core. ANDRILL Southern McMurdo Sound Project, Antarctica.
- Passey B. H., Levin N. E., Cerling T. E., Brown F. H. and Eiler J. M. (2010) High-temperature environments of human evolution in East Africa based on bond ordering in paleosol carbonates. *Proc. Natl. Acad. Sci. USA* 107(25), 11245–11249.
- Passey B. H. and Henkes G. A. (2012) Carbonate clumped isotope bond reordering and geospeedometry. *Earth Planet. Sci. Lett.* 351–352, 223–236.
- Paulsen T., Millan C., Pierdominici S., Wilson T. and Drew S. (2009) Fracture Logging of the AND-2A Core. ANDRILL Southern McMurdo Sound Project, Antarctica, Terra Antartica.
- Paulsen T. S. and Wilson T. J. (2009) Structure and age of volcanic fissures on Mount Morning: a new constraint on Neogene to contemporary stress in the West Antarctic Rift, southern Victoria Land, Antarctica. Geol. Soc. Am. Bull. 121(7–8), 1071–1088.
- Pompilio M., Dunbar N., Gebhardt A., Helling D., Kuhn G., Kyle P., McKay R., Talarico F., Tulaczyk S. and Vogel S. (2007) Petrology and Geochemistry of the AND-1B Core. ANDRILL McMurdo Ice Shelf Project, Antarctica.
- Rennie V. C. F. and Turchyn A. V. (2014) The preservation of  $\delta^{34} S_{SO4}$  and  $\delta^{18} O_{SO4}$  in carbonate-associated sulfate during marine diagenesis: a 25 Myr test case using marine sediments. *Earth Planet. Sci. Lett.* **395**, 13–23.
- Salem A. M., Morad S., Mato L. F. and Al-Aasm I. (2000) Diagenesis and reservoir-quality evolution of fluvial sandstones during progressive burial and uplift: evidence from the Upper Jurassic Boipeba Member, Reconcavo Basin, Northeastern Brazil. AAPG Bull. 84(7), 1015–1040.

- Schauble E. A., Ghosh P. and Eiler J. M. (2006) Preferential formation of <sup>13</sup>C<sup>-18</sup>O bonds in carbonate minerals, estimated using first-principles lattice dynamics. *Geochim. Cosmochim. Acta* **70**(10), 2510–2529.
- Schrag D. P., DePaolo D. J. and Richter F. M. (1995) Reconstructing past sea surface temperatures: correcting for diagenesis of bulk marine carbonate. *Geochim. Cosmochim. Acta* 59 (11), 2265–2278.
- Schröder H., Paulsen T. and Wonik T. (2011) Thermal properties of the AND-2A borehole in the southern Victoria Land Basin, McMurdo Sound, Antarctica. *Geosphere* 7(6), 1324–1330.
- Sharma T. and Clayton R. N. (1965) Measurement of O<sup>18</sup>/O<sup>16</sup> ratios of total oxygen of carbonates. *Geochim. Cosmochim. Acta* **29**(12), 1347–1353.
- Starinsky A. and Katz A. (2003) The formation of natural cryogenic brines. *Geochim. Cosmochim. Acta* 67(8), 1475–1484.
- Staudigel P. T. and Swart P. K. (2016) Isotopic behavior during the aragonite-calcite transition: implications for sample preparation and proxy interpretation. *Chem. Geol.* 442, 130–138.
- Sun T., Socki R. A., Bish D. L., Harvey R. P., Bao H., Niles P. B., Cavicchioli R. and Tonui E. (2015) Lost cold Antarctic deserts inferred from unusual sulfate formation and isotope signatures. Nat. Commun. 6, 7579.
- Swart P. K., Burns S. and Leder J. (1991) Fractionation of the stable isotopes of oxygen and carbon in carbon dioxide during the reaction of calcite with phosphoric acid as a function of temperature and technique. *Chem. Geol.: Isotope Geosci. Sect.* 86(2), 89–96.
- Tang J., Dietzel M., Fernandez A., Tripati A. K. and Rosenheim B. E. (2014) Evaluation of kinetic effects on clumped isotope fractionation (Δ<sub>47</sub>) during inorganic calcite precipitation. *Geochim. Cosmochim. Acta* 134, 120–136.
- Toyota T., Smith I. J., Gough A. J., Langhorne P. J., Leonard G. H., Van Hale R. J., Mahoney A. R. and Haskell T. G. (2013)
  Oxygen isotope fractionation during the freezing of sea water.
  J. Glaciol. 59(216), 697–710.
- Tripati A. K., Eagle R. A., Thiagarajan N., Gagnon A. C., Bauch H., Halloran P. R. and Eiler J. M. (2010) <sup>13</sup>C–<sup>18</sup>O isotope signatures and 'clumped isotope' thermometry in foraminifera and coccoliths. *Geochim. Cosmochim. Acta* **74**(20), 5697–5717.
- Vinn O., Ten Hove H. A., Mutvei H. and Kirsimaee K. (2008) Ultrastructure and mineral composition of serpulid tubes (Polychaeta, Annelida). Zool. J. Linn. Soc. 154(4), 633-650.
- Walcott R. (1970) Isostatic response to loading of the crust in Canada. Can. J. Earth Sci. 7(2), 716–727.
- Wang Z., Schauble E. A. and Eiler J. M. (2004) Equilibrium thermodynamics of multiply substituted isotopologues of molecular gases. *Geochim. Cosmochim. Acta* 68(23), 4779–4797.
- Wonik T., Grelle T., Handwerger D. A., Jarrard R. D., McKee A., Patterson T., Paulsen T., Pierdominici P., Schmitt D. and Schröder H. (2008) Downhole measurements in the AND-2A borehole, ANDRILL southern McMurdo Sound Project, Antarctica. *Terra Antartica* 15(1), 57–68.
- Worley B., Cooper A. and Hall C. (1995) Petrogenesis of carbonate-bearing nepheline syenites and carbonatites from Southern Victoria Land, Antarctica: origin of carbon and the effects of calcite-graphite equilibrium. *Lithos* **35**(3), 183–199.
- Zaarur S., Affek H. P. and Brandon M. T. (2013) A revised calibration of the clumped isotope thermometer. *Earth Planet*. Sci. Lett. 382, 47–57.